Pathogenic mechanisms underlying adverse neurodevelopmental outcome in congenital heart disease

Running Title: Brain Deficits in Congenital Heart Disease

George C. Gabriel[1], Hisato Yagi[1], Tuantuan Tan[1], Abha Bais[1], Benjamin J. Glennon[1], Margaret C. Stapleton[1], Lihua Huang[2], William T. Reynolds[1], Marla G. Shaffer[1], Xinxiu Xu[1], Madhavi Ganapathiraju[3], Dennis Simon[4], Ashok Panigrahy[5], Yijen L. Wu[1], Cecilia W. Lo[1]

(1) Department of Developmental Biology, University of Pittsburgh
(2) Chinese University of Hong Kong
(3) Department of Biomedical Informatics, University of Pittsburgh
(4) Department of Critical Care Medicine, University of Pittsburgh
(5) Department of Radiology, University of Pittsburgh Medical Center

*Correspondence to: Cecilia W. Lo, PhD, Department of Developmental Biology, University of Pittsburgh School of Medicine, 530 45th Street, 8162 Rangos Research Center, Pittsburgh, PA 15201 Email: cel36@pitt.edu

The authors have declared that no conflict of interest exists.

Abstract

Background: Hypoplastic left heart syndrome (HLHS), a severe congenital heart disease, is associated with poor neurodevelopmental outcomes, microcephaly, reduced cortical brain volume, brain dysmaturation, and neurobehavioral disorders such as autism. The involvement of patient intrinsic factors was indicated, but the mechanism is largely unknown.

Methods: *Ohia* mice with HLHS causing mutations in chromatin modifier Sin3A-associated protein 130 (*Sap130*) and cell adhesion protein ProtocadherinA9 (*Pcdha9)* were investigated for brain abnormalities by histology, immunomicroscopy, and molecular profiling by RNAseq, Sap130 ChIPseq, and genome-wide methylome analysis. Additionally, adult viable *Pcdha9*$^{m/m}$ and *Emx1-cre:Sap130*$^{f/-}$ mice with forebrain deletion of *Sap130* were examined by brain MRI and behavioral assessments.

Results: *Ohia* mice have brain abnormalities comprising forebrain hypoplasia and microcephaly in conjunction with a cortical neurogenesis defect. This is associated with loss of intermediate progenitors due to mitotic arrest and apoptosis from multipolar spindle formation, a mechanism also observed in primary microcephaly. Brain RNAseq showed perturbation of REST transcriptional regulation of neurogenesis, disruption of CREB signaling regulating synaptic plasticity and memory, and defects in neurovascular coupling indicating perturbation of brain-sparing cerebral autoregulation. Disease pathways recovered included autism, intellectual disability, and other neurobehavioral/neurological deficits. These same pathways were observed upon intersection of genes that are differentially expressed with those that are differentially methylated and also are ChIPseq targets of Sap130, suggesting the transcriptional changes are epigenetically regulated. Adult viable mice harboring either the *Pcdha9* mutation or forebrain-specific *Sap130* deletion showed similar learning/memory deficits and autism-like behavior, suggesting they act on convergent pathways.

Conclusions: Our observations indicate the intrinsic factors contributing to the adverse neurodevelopmental outcome associated with HLHS involve spindle defects causing impaired corticoneurogenesis, and brain and behavioral deficits associated with perturbed epigenetic regulation of neurodevelopmental pathways.

Novelty and Significance

What is known?

- Hypoplastic left heart syndrome (HLHS), a severe congenital heart disease, is associated with adverse neurodevelopmental outcome attributable to patient intrinsic factors.
- Cortical neurogenesis defect with reduced brain volume and microcephaly are observed beginning *in utero,* suggesting a developmental etiology.
- Learning impairment and autism spectrum disorder are commonly observed in HLHS.

What new information does this article contribute?

- The *Ohia* HLHS mouse model exhibits neurodevelopmental deficits comprising microcephaly and cortical neurogenesis defects with loss of neural progenitors from multipolar spindle formation, as well as impaired neurovascular coupling.
- Molecular profiling showed disturbance of REST, transcriptional regulator of neural stem cells, and CREB signaling regulating synaptic plasticity, with neurobehavioral assessments of the mutant mice showing learning/memory and autism-like behavioral deficits.
- Intersection of transcriptome and DNA methylation analyses uncovered an epigenetic basis for the neurodevelopmental/neurobehavioral abnormalities,

Analysis of an HLHS mouse model indicated patient intrinsic factors causing adverse neurodevelopment in HLHS are genetic and epigenetic in etiology. This may include a mitotic spindle defect that would not be rescued by in utero aortic

valvuloplasty, and a defect in neurovascular coupling that is likely to reduce the efficacy of maternal hyperoxygenation. However, epigenetic therapy may provide a new avenue for treatment that should be explored.

Introduction

Congenital heart disease affects up to 1% of live births, and with surgical and medical advances, there are now more adults with CHD than infants born annually with CHD[1,2]. However, CHD survivors often suffer developmental delay with high risk of neurodevelopmental impairment that can significantly degrade quality of life[3]. This is associated with a "neurobehavioral signature" that includes learning disabilities, impaired social/communication skills, autism spectrum disorders, and other cognitive, behavioral and neuropsychiatric deficits[3,4]. While the major contributing factors were previously thought to be hypoxic injury and complications from multiple congenital cardiac surgeries, outcome studies have pointed to patient intrinsic factors playing a prominent role in determining neurodevelopmental outcome[4-7]. This is supported by the finding of small head circumference, brain abnormalities, and various neurobehavioral deficits even before cardiac surgery[8-11]. That these patient intrinsic factors may encompass genetic factors is suggested by the fact that chromatin modifiers previously demonstrated to contribute to the genetic etiology of CHD are also known to cause autism, intellectual disability, cognitive impairment, and neuropsychiatric disorders[12-14]. In addition, other patient-specific factors such as known genetic disorders and socioeconomic status increase risk for adverse neurodevelopmental outcomes in CHD[15,16].

Among patients with CHD, the highest morbidity and mortality is observed in patients with hypoplastic left heart syndrome (HLHS), a severe CHD now survivable with a three-stage surgical palliation. However, HLHS survivors have high risk of neurodevelopmental delay and neurobehavioral and cognitive impairment[3]. This is associated with reductions in functional status and quality of life, increase in behavioral symptoms, poor adaptive skills required for navigating school and daily living, and intellectual disability with deficits in full scale IQ[17-19]. HLHS is also associated with impaired brain development. Microcephaly, holoprosencephaly, and agenesis of the corpus callosum are observed in 25% of HLHS fetuses[3,11]. Microcephaly was shown to predict early adverse neurologic outcomes[20]. While the brain volume reductions show correlation with

lower cerebral substrate delivery, neurodevelopmental outcome was not improved after in utero fetal intervention with aortic valvuloplasty, suggesting involvement of intrinsic brain defects[21].

To investigate the potential causes of poor neurodevelopment in HLHS we pursued studies using the *Ohia* mouse model of HLHS. This mouse model was recovered from a large scale forward genetic screen for CHD and found to harbor two recessive mutations that in combination cause HLHS, Sin3A-associated chromatin modifier *Sap130,* and protocadherin cell adhesion protein *Pcdha9* from the α-protocadherin gene cluster[22]. Both the Sin3A complex and the clustered protocadherins have essential roles in development of the nervous system. The Sin3A protein is part of the histone deacetylase (HDAC) repressor complex known to play critical roles in brain development, and *SIN3A* deficiency in humans causes Witteveen-Kolk syndrome associated with intellectual disability, autism, microcephaly, and facial dysmorphism[23]. Also found in the Sin3A complex is MECP2, an X-linked methyl CpG binding protein associated with Rett syndrome, the most common cause of cognitive impairment in females[24]. The clustered protocadherins are essential for development of the nervous system. They provide cell surface diversity encoding neuronal identity regulating synaptic connectivity in the brain[25]. Mice with deletion of the entire *Pcdha* gene cluster exhibit deficits in synaptic connectivity and behavior[26]. Mutations in both *PCDHA* and *SIN3A* are clinically implicated in autism[23,27].

Leveraging the *Ohia* mouse model, we examined impact of the *Sap130/Pcdha9* mutations on development of the brain with histopathological analysis and immunohistology. Molecular profiling was conducted using RNA sequencing (RNAseq) and Sap130 chromatin immunoprecipitation sequencing (ChIPseq). Genome wide DNA methylation was also investigated, as the Sin3A complex has been shown to interact with the Tet family of methylcytosine dioxygenases to regulate DNA methylation (DNAm)[28]. DNAm changes are also well described to play a role in neurodevelopmental/neuropsychiatric disorders[29,30]. To further investigate the specific role of *Sap130* in the brain abnormalities, we used a floxed *Sap130* allele and Emx1-Cre to generate mice with forebrain-specific deletion of *Sap130*. As the latter mice and

mice harboring only the *Ohia Pcdha9* mutation are adult viable, we further conducted neurobehavioral assessments. Together these studies yielded new insights into the pathogenic mechanisms contributing to the poor neurodevelopment in HLHS.

METHODS

Extended, more detailed methods are provided in the Supplemental Material. All data supporting the findings of this study are available from the corresponding author upon reasonable request.

Mouse Husbandry Mouse studies were conducted under a University of Pittsburgh Institutional Animal Care and Use Committee approved animal study protocol. *Ohia* and *Pcdha9* (c.2389_2399del; [p.Asp796Phefs∗]) mice generated by CRISPR gene editing were maintained in the C57BL/6J background. B6.129S2-Emx1tm1(cre)Krj/J mice with *Emx1-cre* driver were purchased from Jackson Laboratory (Strain #005628) and intercrossed with *Sap130*$^{f/f}$ and *Sap130*$^{+/-}$ mice generated previously[22].

Immunostaining and Confocal Microscopy *Ohia*$^{m/m}$ fetuses were fixed in 4% PFA overnight, and cryoembedded. Cryosections were generated and stained with different antibodies to various neural markers (see Supplemental Methods). Human induced pluripotent stem cell derived cardiomyocytes (iPSC-CMs) from four HLHS patients were fixed in 4% paraformaldehyde and stained with antibody against 5-methylcytosine (Active Motif, RRID: AB_2687950)[31]. Confocal imaging was conducted with the Leica SP8 confocal microscope and quantitatively analyzed with ImageJ.

Mouse Embryonic Fibroblast Analysis MEFs were isolated from E14.5-E15.5 embryos as previously described, with three independent MEF lines analyzed. Cells were plated on glass coverslips, fixed in 4% PFA, stained with antibodies to α-tubulin (Abcam; ab15246), and γ-tubulin (Sigma; T6557) and counterstained with DAPI (Thermo Fisher Scientific; D1306).

Histological Reconstructions Using Episcopic Confocal Microscopy E14.5 or newborn mice were euthanized, the heads embedded in paraffin for episcopic confocal microscopy (ECM) as previously described[22]. The 2D serial ECM image stacks collected are digitally resliced and also 3D reconstructed using the OsiriX Dicom viewer (https://www.osirix-viewer.com) to assess brain anatomical structures.

RNA Sequencing RNA sequencing of brain tissue was conducted using standard protocols on Illumina HiSeq 2000 (BGI Americas) with 100-bp paired-end reads, and using standard bioinformatics pipeline (see Supplemental Methods) and aligned to mm10 (NCBI build 38). Differential expression analyses were performed with edgeR, and differentially expressed genes for *Ohia*$^{m/m}$ mutant brain were identified with FDR $\leq$0.05 (Benjamini–Hochberg), and for *Emx1-cre*:*Sap130*$^{f/-}$ with FDR<0.1. Pathway analysis was carried out genes identified to be differentially expressed.

Chromatin Immunoprecipitation Sequencing Sap130 chromatin immunoprecipitation was performed with rabbit anti-Sap130 antibody (A302-491A, Bethyl laboratories) and an iDeal ChIP–seq Kit for Transcription Factors (Diagenode) as previously described[22] (see Supplemental Methods). Reads were aligned to mm10 and Sap130 target regions were identified with MACS1.4.2. Motif enrichment analysis was performed using MEME suite version 5.4.1.

Methylation Analysis Methylation analysis was conducted using the Illumina Infinium mouse methylation beadchip using standard protocol (see Supplemental Methods).

Probes with FDR$\leq$0.1 were considered significantly differentially methylated. Differentially methylated regions (DMRs) were identified using the DMRcate (v 2.4.1) with FDR of 0.05.

Mouse Behavioral Phenotyping Mouse behavior was assessed using three training paradigms: the Morris water maze, fear conditioning, and sociability. Testing was completed by operator blinded to genotype. See Supplemental Methods for more details.

Magnetic Resonance Imaging Following behavioral testing, mice underwent in vivo brain MRI carried out using a Bruker BioSpec 70/30 USR spectrometer (Bruker BioSpin MRI, Billerica, MA, USA) operating at 7-Tesla with quadrature radio-frequency volume coil with inner-diameter of 35 mm.

Statistical Analysis: Data were analyzed using GraphPad Prism 9 (GraphPad Software). For cell quantification independent samples T-test was used (*$p<0.05$). For mouse behavioral analysis, data were analyzed by two-way, two-way repeated measures, or three-way analysis of variance (ANOVA).

Results

Ohia mutant mice double homozygous for the *Sap130/Pcdha9* mutations (*Ohia*$^{m/m}$) were previously shown to exhibit HLHS and other CHD with incomplete penetrance[22]. Head defects can also be observed, with analysis of 83 newborn pups showing 56.7% with craniofacial defects, 48.2% exhibiting both CHD and craniofacial defects, and 8.5% with only craniofacial defects, while 24% showed only CHD. These findings show incomplete penetrance of the head and heart defects. The craniofacial defects also were variable in severity, ranging from mild micrognathia to severe agnathia, often accompanied by low set ears, dome shaped head, and eye defects (Figure S1).

Examination of gross brain anatomy in *Ohia* mice (n=40) from E14.5 to E18.5 revealed 81% have forebrain hypoplasia, with 59% exhibiting severe microcephaly (Figure 1A-D). In approximately half of the severe cases (49.6%), holoprosencephaly was observed. Analysis of severe mutants using episcopic confocal microscopy (ECM) for serial section histological analysis and high-fidelity 3D reconstructions revealed hypoplastic/aplastic olfactory bulbs, thin cerebral cortex, hypoplasia of the cerebellum, reduction of cerebellar fissures, dilation of the lateral ventricles, and hypoplasia of the corpus callosum (Figure 1E-J). Quantification confirmed significant cortical thinning, indicating defects in cortical plate formation (Figure 1K-N).

Impaired Cortical Neurogenesis with Reduction of Intermediate Progenitors

Cortical plate formation is orchestrated via the expansion of neural progenitors in the ventricular and subventricular zone. These progenitors give rise to cells that migrate upwards to form layers II through VI of the cortical plate, with layer VI being the innermost layer which is also the first to form and the outermost Layer II being the last to form. Immunostaining using antibodies for different progenitor lineages and for different layers of the cortical plate showed no change in Pax6+ apical progenitors (radial glial cells) in the ventricular zone, but Tbr2+ intermediate progenitors in the subventricular zone were markedly reduced (Figure 2A-L). Satb2, a marker for postmitotic neurons in the upper layers of the developing cortex, was also markedly reduced,

indicating failure to form the later born neurons in layers II-IV in the *Ohia*$^{m/m}$ brain (Fig 2M-P vs. Q-T, quantified in Fig 2U-Y). In contrast, the Tbr1+ earlier born neurons of layers VI, and Ctip2+ neurons in layer V-VI were present, but abnormally distributed in overlapping domains as compared to their normal pattern of deployment in wildtype mice (Figure 2Q-T vs. M-P). These observations indicate a cortical neurogenesis defect involving failure of the intermediate progenitors to expand, thereby causing deficiency in the later born neurons in layers II-IV.

Loss of Neural Progenitors Associated with Mitotic Block

To elucidate the mechanism of the cortical neurogenesis defect in the *Ohia*$^{m/m}$ brain, we quantified cell proliferation and apoptosis. Analysis of E14.5 *Ohia*$^{m/m}$ brain tissue showed a significant increase in pH3 positive cells in the subventricular zone, and also increased TUNEL throughout the ventricular and subventricular zones (Figure 3A-F, quantified in G), findings reminiscent of those seen in the *Ohia*$^{m/m}$ HLHS heart tissue[22]. The fraction of mitotic cells in anaphase/telophase decreased, indicating metaphase block (Figure 3H)[22]. Similar findings have been reported in primary microcephaly and are associated with mitotic spindle defects, such as with mutations in *ASPM*, Assembly Factor for Spindle Microtubules, and *WDR62*, another centrosome/spindle protein, two genes that account for over 50% of primary microcephaly[32,33].

To investigate for spindle defects, mouse embryonic fibroblasts (MEFs) derived from *Ohia*$^{m/m}$ mutant embryos and littermate controls were immunostained for α-tubulin to visualize the spindle apparatus and γ-tubulin for the centrosome. This revealed a marked increase in multi-polar spindles in the *Ohia*$^{m/m}$ MEFs that are seldom seen in wildtype MEFs (Figure 3L-N vs. 3I-K, quantified in 3O). This was associated with an increase in mitotic cells at prophase/metaphase (P/M) and concomitant decrease in anaphase/telophase (A/T), confirming mitotic block (Figure 3P). Amongst cells in anaphase, a much higher incidence of lagging chromosomes was observed (Figure 3Q, R). Together these findings support a spindle defect contributing to the loss of later born neurons in cortical layers II-IV and the emergence of microcephaly in *Ohia*$^{m/m}$ mice.

Dysregulated Gene Expression and Defects in Neurodevelopment

Transcriptome profiling was conducted with RNAseq analysis of E13.5-E14.5 brain from *Ohia*$^{m/m}$ mutants (n=3) and wildtype littermate controls (n=5). This yielded 1,549 differentially expressed genes (DEGs), 1,081 downregulated and 468 upregulated (FDR 0.05; Supplemental Dataset 1). Metascape analysis of the DEGs yielded many nervous system related terms, including forebrain development, forebrain generation of neurons, synapse assembly, axon guidance, action potential, glutamatergic synapses, ion transport, and learning and memory (Figure 4A). Ingenuity Pathway Analysis (IPA) of the DEGS for upstream regulators and downstream pathways recovered as upstream regulators, REST - repressor element 1 silencing transcription factor, which was upregulated, DTNBP1 - dystrobrevin binding protein 1, and SGK1 - serum glucocorticoid regulated kinase 1, both down regulated (Supplemental Dataset 1). The recovery of REST is particularly notable in the context of microcephaly, as REST is known to control expansion of neural progenitors via recruitment of HDACs to the Sin3A complex to repress transcription of proneuronal genes, including the GRIN family of glutamate receptors, which are downregulated in the *Ohia* mutant brain (Figure 4B)[34]. DTNBP1 regulates neurotransmitter release and receptor signaling and is linked to cognitive impairment and schizophrenia, while SGK1 regulates glutamate receptor expression and facilitates spatial learning and hippocampal long-term potentiation[35-37]. The downstream biological processes predicted to be impacted by the transcriptomic changes in this upstream-downstream analyses are all neurobehavioral related, including learning, long-term potentiation, coordination, conditioning, analgesia, hyperalgesia (Figure 4B).

IPA canonical pathway analysis also recovered cyclic AMP response element binding protein (CREB) signaling, synaptic depression/potentiation, synaptogenesis signaling, GABA receptor signaling, and calcium signaling (Figure 4C; Supplemental Dataset 1). Associated with the CREB signaling pathway is the reduction in glutamate receptor signaling and downregulation of PKC, PLC, PKA, calmodulin, and CAMKII/CAMK4 (Figure 4D). This pathway has critical roles

in synaptic plasticity mediating long term memory, and is involved in the pathogenic alteration of synaptic plasticity and memory associated with neurocognitive disorders and various neurodegenerative diseases such as Alzheimer's Disease and Huntington's disease, and implicated in schizophrenia and depressive disorders[38]. ToppGene disease pathway enrichment analysis identified autism, mental depression, intellectual disability, seizures, various neuropsychiatric diseases such as schizophrenia and bipolar disorder, and also recovered was neurodegenerative diseases (Figure 4E, Supplemental Dataset 1). Interestingly, we also observed circadian rhythm, which may reflect the known role of CREB in circadian rhythm regulation[39].

Perturbation of Neurovascular Coupling Involving Defect in Nitric Oxide Signaling

The top IPA pathway recovered from the *Ohia* mutant brain RNAseq analysis was neurovascular coupling, an autoregulatory mechanism by which the brain's energy demands are closely coordinated with cerebral blood flow (Figure 4C)[40]. This regulation is mediated by neuronal activity dependent production of nitric oxide (NO), which promotes relaxation of vascular smooth muscle, causing dilation of cerebral arteries to increase blood flow to the brain. In the *Ohia* mutant brain, there is marked reduction in the expression of transcripts for nitric oxide synthase (NOS, see blue asterisks, Figure 5), indicating such autoregulation may be impaired. The downregulation of NOS (FDR=8.03E-14, Supplemental Dataset 1) is observed to be accompanied by reduction of guanylate cyclase and many ion channel proteins regulating neuronal activity and vascular smooth muscle relaxation/contraction (Figure 5). The only gene upregulated is cGMP dependent protein kinase PKG, likely a compensatory response to the reduced NO (Figure 5). Overall, these transcriptional changes would suggest the brain sparing autoregulation often observed with CHD may be impaired in the *Ohia* mutant[41]. We note clinically, such autoregulation has been shown to be impaired in fetuses with HLHS, supporting the present findings in the *Ohia*

mutant mice[42]. Also supporting disturbance of NO signaling is the additional recovery of the IPA pathway, “Effect of sildenafil”, a drug commonly used to promote vasodilation by enhancing NO signaling via the inhibition of phosphodiesterase breaking down cGMP (Figure 4C). NO signaling has additional roles in CREB regulated neuronal gene expression[43] to determine synaptic plasticity in learning/memory.

Chromatin Immunoprecipitation Sequencing Recovers Genes Regulating Neurogenesis

To elucidate how Sap130 may contribute to brain abnormalities in the *Ohia* mutant mice, we conducted chromatin immunoprecipitation sequencing (ChIPseq) analysis with a Sap130 antibody to identify genes that may be subject to Sap130 regulation. ChIPseq analysis of E13.5 wildtype mouse brain tissue recovered 16,231 Sap130 binding sites, with 10,753 situated within 1 kb of transcriptional start sites, identifying the associated genes as possible Sap130 target genes (Supplemental Dataset 2). This included transcription regulators of neurogenesis such as *Rest*, *Sin3A*, *CTCF, Satb2, Klf13,* and also microcephaly-related genes such as *Aspm* and *Wdr62* (Figure 6A). Pathway enrichment analysis of these putative Sap130 target genes yielded GO biological processes comprising chromosome organization, cell cycle progression, and neurogenesis (Figure 6B). Cellular components recovered included mitochondrion, centrosome, glutamatergic synapse and transcriptional regulation (Figure 6C). For human phenotypes, hypoplasia/dysplasia of the cerebrum, reduced head circumference, microcephaly, and intellectual disability were recovered (Figure 6D). Disease pathway yielded some of the same terms as in human phenotype, but additionally, included neurodevelopmental delay, neurodegenerative disorders, epilepsy, autism, and ciliopathies (Figure 6E, Supplemental Dataset 2). Transcription factor binding site analysis identified enrichment for SP, KLF, IRF, ELF, and RFX motifs (Figure 6F). SP and KLF are closely related zinc finger proteins that bind GC rich promoters, and are commonly associated with pluripotency and cell cycle genes[44]. KLF, Kruppel like transcription factors, also are known to have important roles in brain and heart development[45,46]. As neurodevelopmental defects are often seen in ciliopathies, we further

examined ciliogenesis in the *Ohia* mutant brain. A marked reduction in ciliation was observed, supporting an association with ciliopathy (Figure 6G-I).

DNA Methylation and Transcriptional Perturbations in *Ohia* Mutant Brain

Parallel analysis of DNA methylation was conducted using the Illumina Infinium mouse methylome array with probes for over 285,000 CpG sites genome wide[47]. Analysis was conducted on DNA from the forebrain tissue of E15.5 *Ohia*$^{m/m}$ mutant mice (n=3) with microcephaly vs. age matched C57BL/6J wildtype mice (n=3). Total DNA methylation (DNAm) level was observed to be reduced in the *Ohia* mutant mice when compared to that of wildtype controls (Figure 7A). Using a 5-methycytosine antibody, we investigated clinical relevance of these findings by examining DNA methylation in the induced pluripotent stem cell derived cardiomyocytes (iPSC-CM) of four HLHS patients vs. two control subjects. This also showed reduction in total DNAm level in the HLHS patient iPSC-CM (Figure 7B,C).

Analysis of the total beadchip data of the *Ohia* mutant and wildtype mouse brain showed correlation of higher promoter DNAm with lower gene expression (Figure S2). We recovered 5,117 differentially methylated regions (DMRs; FDR<0.05) associated with 4,179 genes (Figure 7E; Supplemental Dataset 3). By way of example, we show CpG methylation associated with two DMRs in *Klf13*, a negative regulator of CREB signaling involved in axonogenesis and neurite outgrowth (Figure 7D)[46]. Marked increase in DNA methylation was observed at the DMR situated at the terminal exon of Klf13, interestingly a genomic region with high sequence conservation across species (Figure 7D).

Intersection of genes associated with the DMR and downregulated DEGs recovered from the RNAseq analysis identified 297 genes (Figure 7E, Supplemental Dataset 4).ToppGene pathway enrichment analysis yielded Mouse Phenotypes related to brain, behavior, and neurological function (Figure 7G, Supplemental Dataset 4), and for Diseases, we observed autism, intellectual disability, and epilepsy, diseases known to be associated with HLHS (Supplemental Dataset 4). No Human Phenotype was recovered in this analysis. In contrast,

intersection of upregulated DEGs with DMRs identified 61 genes, associated with metabolic pathways (Figure S3, Supplemental Dataset 4).

DNA methylation and Sap130 Mediated Transcriptional Regulation

To assess potential impact of the *Sap130* mutation on the epigenetic and transcriptional changes observed in the *Ohia* mutant brain, we conducted additional three-way intersection of the up or downregulated DEGs with the DMR associated and Sap130 ChIPseq genes. With the downregulated DEGs, this three-way intersection yielded 161 genes (Figure 7F), and ToppGene analysis recovered similar Mouse Phenotypes and Diseases as seen with the two-way DMR/DEG intersecting genes, thus indicating that genes contributing to the neurological phenotypes and diseases are likely subject to Sap130 regulation (Figure 7H; Supplemental Dataset 4). In contrast to these findings with the downregulated DEGs, three-way intersection of the upregulated DEGs yielded only 43 genes (Figure S3), and no Mouse Phenotype or Disease terms recovered. Several disease terms associated with neurodevelopmental impairment were found across multiple analyses (Figure 7I). Overall, these findings suggest DNA methylation associated with Sap130 epigenetic regulation underlie the brain and neurological phenotypes and diseases associated with the *Ohia* mutant mice.

Protein-Protein Interactome Network Analysis

To further functionalize genes downregulated and differentially methylated in the *Ohia* brain, STRING-db was used to construct protein-protein interaction (PPI) network (Supplementary Dataset 5). This analysis yielded significant findings with the PPI network assembled from the hypomethylated and downregulated genes (n=127, FDR=0.05; Figure S4). This network comprising 132 genes included 82 of the 127 hypomethylated/downregulated genes and 50 additional genes recovered by STRING-db (Figure S4A; Supplementary Dataset 5). ToppGene analysis yielded significant terms for Mouse Phenotype, Human Phenotype, Diseases, and Pathways. For Human Phenotype, polymicrogyria was retrieved as the top phenotype (Figure S4B), a defect involving abnormal small cortical folds in the forebrain, a phenotype also seen in

human fetuses with HLHS and in primary microcephaly[42,48]. Also observed were multiple seizure related terms, and abnormal hippocampal morphology (Figure S4B). For Mouse Phenotype, this yielded terms such as cerebral hemisphere morphology, abnormal forebrain morphology, abnormal neuron morphology, abnormal inhibitory postsynaptic currents, terms not seen with analysis of the DMR/DEG intersecting genes alone (Figure S4C). Disease terms recovered included several that overlapped those seen with the DMR/DEG analysis, such as neurodevelopmental disorder, autism, impaired cognition, and epilepsy (Figure S4D). Interestingly, from Pathway enrichment, multiple cilia related terms were recovered, with the top pathway being "cargo targeting to cilium", and also "cargo trafficking to periciliary membrane" and "cilium assembly" (Figure S4E). Together these findings point to the disturbance of ciliogenesis, consistent with the reduced ciliation observed in the *Ohia* mutant forebrain (Figure 6G-I).

Forebrain Specific Deletion of *Sap130* Causes Microcephaly

The histological analysis and molecular profiling of *Ohia*$^{m/m}$ fetal mice showed microcephaly associated with prominent forebrain defects. To investigate if these defects may be cell autonomous and specific to requirement of *Sap130* in the forebrain, we generated a floxed allele of *Sap130* and intercrossed it into mice carrying Emx1-Cre to target forebrain specific deletion of *Sap130*. This Cre driver is expressed in excitatory neurons and glia in the developing cerebral cortex from E9.5 onwards[49]. We observed the Emx1-Cre:*Sap130*$^{f/-}$ mice do not exhibit CHD, and are adult viable. Nevertheless, they have microcephaly with prominent reduction in forebrain size (Figure 8A), which was confirmed with measurement of the brain/body weight ratio (Figure 8B). Real time PCR analysis showed marked reduction in *Sap130* transcripts in the forebrain (Figure 8C). Interestingly, the microcephaly in the Emx1-Cre:Sap13$^{f/-}$ mice showed complete penetrance, unlike the *Ohia*$^{m/m}$ mice. Among the 28 genes known to cause primary microcephaly, many of which are centrosome related, four were up regulated in the Emx1-Cre:*Sap130*$^{f/-}$ forebrain (*Wdr62*, *Cit, Ncapd2, Pcnt)* (Figure 8D; Supplemental Dataset 6). Centrosome amplification can cause spindle defects and is one of the pathogenic mechanisms

known to cause microcephaly[50]. These findings indicate a cell autonomous requirement for *Sap130* in the forebrain in regulating expansion of neural progenitors.

RNAseq analysis of the E14.5 forebrain of *Emx1-cre*:*Sap130*$^{f/-}$ mice (n=3) and littermate controls (n=3) recovered 369 DEGs, 202 down and 167 upregulated (FDR<0.1; Supplemental Dataset 6). IPA pathway enrichment analysis of the DEGs identified axonal guidance as the top pathway, followed by cell cycle, Wnt signaling, and semaphorin signaling in neurons (Figure 8E). Also observed were GADD45 signaling, a stress activated pathway induced with DNA damage and cell cycle checkpoint control, DNA break repair, and HOTAIR regulation - a lncRNA regulating cell cycle and apoptosis via epigenetic gene silencing by providing a scaffold for chromatin remodeling with recruitment of REST/Co-REST and lysine demethylase LSD1, proteins in the Sin3A complex. Further analysis for gene set enrichment also recovered “Centrosome” and “Mitotic Spindle”, further supporting mitotic spindle defects (Figure 8F). In addition, “Hypoxia” was recovered in the gene set enrichment analysis, an unexpected finding given the Emx1-Cre deletion mice do not have CHD. Mouse Phenotype terms recovered included abnormal neuronal differentiation, abnormal forebrain morphology, abnormal limbic system, small olfactory bulb, abnormal neural precursor, abnormal social interaction and abnormal neocortex (Figure 8G). For “Disease” enrichment, intellectual disability was recovered as the top pathway, and also recovered were impaired cognition, neurodevelopmental disorders, microcephaly, and autism (Figure 8H), results overlapping with transcriptomic changes observed in the *Ohia* mutant brain. Also recovered were cerebrovascular accidents and hypoxic-ischemic encephalopathy, supporting the finding of hypoxia. Together these findings suggest microcephaly in *Ohia* mutants is not secondary to CHD, but may reflect the cell autonomous requirement for *Sap130* for normal forebrain neurodevelopment.

Adult *Pcdha9*$^{m/m}$ and Emx1Cre Deleted *Sap130* Mice Exhibit Behavioral Deficits

The molecular profiling of the developing *Ohia*$^{m/m}$ fetal brain predicts impaired cognitive function with possible learning/memory defects and autism spectrum disorder. To assess for

these neurobehavorial deficits, we generated adult viable mice homozygous for the *Pcdha9* mutation, and also mice Emx1-Cre:*Sap130*$^{f/-}$ mice with forebrain deletion of *Sap130* as described above. Brain anatomy of the *Emx1-cre:Sap130*$^{f/-}$ and *Pcdha9*$^{m/m}$ adult mice were analyzed using brain MRI. The *Emx1-cre: Sap130*$^{f/-}$ mice showed significant reduction in total forebrain volume, and volume of the corpus callosum, cortex, and hippocampus (Figure 9A-F). In the *Pcdha9* mutant mice, only mild hippocampal dysplasia was observed but no other appreciable changes in brain structure or size (Figure 9G,H). Neurobehavioral phenotypes were further assessed using three tests to evaluate spatial learning and memory, fear associative learning, and sociability. These tests were administered on 18 female and 6 male *Pcdha9*$^{m/m}$ mice and 6 male and 3 female *Emx1-cre*:*Sap130*$^{f/-}$ mice. For the *Pcdha9*$^{m/m}$ mice, equal number of sex and age matched C57BL/6J wildtype mice were assessed as controls. For the *Emx1-cre*:*Sap130*$^{f/-}$ mice, littermate controls were used comprising Emx1-Cre:*Sap130*$^{f/+}$ mice and *Sap130*$^{f/+}$ mice without Emx1-cre.

Spatial learning and memory were interrogated using the Morris water maze whereby mice are trained to find a hidden platform in a pool of water. After training, no significant difference in the time (latency) required to find the hidden platform was observed for either the *Pcdha9*$^{m/m}$ or Emx1-Cre:*Sap130*$^{f/-}$ mice (Figure 9I,J, Figures S5,S6). In the fear conditioning test, mice learn to associate a cue (a tone) with an adverse event (foot shock) administered after the cue. After training, mice typically freeze when they hear the cue, but return to normal activity post cue. Emx1-Cre:*Sap130*$^{f/-}$ mice and *Pcdha9*$^{m/m}$ female, but not male mice, showed increased post-cue freezing, indicating impaired associative learning (Figure 9K,L; Figures S5,S6). We also conducted sociability testing in which mice are presented with a novel object vs. a novel mouse. While wildtype and littermate control mice showed preference for the novel mouse (Figure 9M,N), Emx1-Cre:*Sap130*$^{f/-}$ mice and *Pcdha9*$^{m/m}$ female, but not male mice, showed equal time spent exploring the novel object and novel mouse (Figure 9M,N, Figures S5,S6), indicating autism-like social interaction deficits. It was not possible to assess gender effects in the Emx1-Cre:*Sap130*$^{f/-}$ mice given the smaller cohort size.

DISCUSSION

CHD patients, most of whom now survive to adulthood, are at high risk of adverse neurodevelopmental outcome that can significantly degrade their quality of life. Our studies of *Ohia* mice with mutations causing HLHS revealed a cortical neurogenesis defect associated with microcephaly, impaired neurovascular coupling and neurobehavioral deficits, phenotypes associated with HLHS. This is congruent with the finding that many genes highly expressed in the heart are also highly expressed in the brain[12]. Also notable, a substantial fraction of de novo pathogenic mutations recovered from CHD patients are in genes associated with neurodevelopmental disabilities (NDD)[12]. The forebrain hypoplasia and microcephaly observed in *Ohia* mice are reminiscent of the brain volume reduction observed clinically with in utero imaging and is closely correlated with reduction in fetal brain oxygenation[51-53]. These findings are in line with our transcriptome profiling indicating a defect in "neurovascular coupling". A reduction in nitric oxide synthase is also observed, predicting a disruption in cerebral autoregulation, a circuit observed in CHD fetuses shunting blood to the brain to improve fetal brain oxygenation[41]. Indeed, impaired cerebral autoregulation has been suggested by a clinical study of fetuses with evolving HLHS[42]. Using measurement of nasal NO (nNO) as a surrogate measure for intrinsic NO production capacity we previously showed HLHS patients have low nNO, and hence likely low NO production capacity[54]. Follow up blood oxygen level dependent (BOLD) brain MRI showed CHD patients with low nNO also have impaired neurovascular coupling, and also impaired cognitive function[55]. We noted the brain transcriptome profiling of Emx1-Cre:*Sap130*$^{flx/-}$ mouse forebrain yielded "hypoxic-ischemic encephalopathy" and "cerebrovascular accident", suggesting neurovascular coupling defect arising from *Sap130* deficiency in the brain alone.

We showed the forebrain hypoplasia and microcephaly are likely the result of a cortical neurogenesis defect from loss of later born neurons in cortical layers II-IV. Previous clinical MRI study of human fetuses with HLHS also uncovered a cortical neurogenesis defect associated with volume reduction in the cortical subplate, intermediate and ventricular zone[56]. Our transcriptome

analysis indicated the disturbance of REST, a master transcriptional regulator that recruits HDACs to the Sin3A complex to epigenetically regulate neural progenitor expansion and neural stem cell maintenance[57-60]. HDAC deficiency in mice can cause microcephaly with similar loss of intermediate progenitors from the perturbation of REST[61]. Mutations in *ZNF335,* another component of the Sin3A complex required for REST regulation of neurogenesis can cause a clinically extreme form of microcephaly[62]. Together these findings indicate the Sin3A complex and Sap130 play an essential role in cortical neurogenesis.

At the cellular level, we observed the loss of intermediate progenitors is associated with apoptosis likely mediated by metaphase block and mitotic check point activation from multipolar spindle formation. Consistent with this, “centrosome” and “mitotic spindle” were recovered from gene set enrichment analysis of the Emx1-Cre:*Sap130*$^{flx/-}$ forebrain transcriptome, and “cell cycle” and “centrosome” were recovered from the Sap130 ChIPseq analysis. These findings suggest centrosome function is subject to Sap130 regulation. Multipolar spindle formation is a pathogenic mechanism known to cause primary microcephaly, such as with mutations in *Wdr62*, one of the major genetic causes of microcephaly[63]. Interestingly, elevated expression of *Wdr62* and several other microcephaly associated centrosomal genes was observed in *Ohia* mutant brain, indicating possible centrosome amplification, a pathogenic mechanism also associated with primary microcephaly[50,64].

We observed a ciliogenesis defect in *Ohia* brain cortex that may reflect secondary defect involving the basal, which is centrosome derived, and provides the template for ciliogenesis. As primary cilia also transduce cell signaling regulating interneuronal connectivity, cilia defects have been proposed to cause circuit malformations in ciliopathies[65]. The finding of holoprosencephaly among *Ohia* mutants and HLHS patients would suggest possible perturbation of cilia transduced hedgehog signaling[66]. Particularly notable is recovery of “ciliopathy” as a significant disease pathway from the Sap130 ChIPseq analysis. Clinically, HLHS has been observed in association with various ciliopathies, with one study showing increased burden for ciliopathy related sequence

variants in HLHS patients[67,68]. Multiple other cilia-related pathways were also recovered in the PPI network analysis.

We also observed the disturbance of CREB signaling, a cAMP and calcium responsive transcriptional pathway regulating neuronal plasticity, learning and memory, long term potentiation and the encoding of long-term memory. As CREB also can be modulated by NO, NO deficiency can exacerbate CREB associated neurological deficits[43]. CREB perturbation would predict cognitive impairment and also memory related diseases such as Alzhemier's[38]. HLHS and other single ventricle CHD patients have hazards ratio of 2.6 (95% CI:1.8-3.8) for early onset dementia[38,69]. CREB signaling also regulates dopaminergic neurons implicated in autism, and CREB disturbance has been associated with Timothy syndrome, a disorder with high penetrance for autism[70]. Our mouse behavioral assessment identified impairment in contextual learning/memory and also autism-like social interaction deficits. Surprisingly the same defects were observed in both the Emx1-Cre:*Sap130*$^{f/-}$ and *Pchda9* mutant mice. Disease pathway enrichment of the transcriptome profile from the Emx1-Cre:*Sap130*$^{f/-}$ mouse forebrain yielded intellectual disability, impaired cognition and autism. Disturbance of REST transcriptional regulation and altered CREB signaling can contribute to these behavioral deficits via perturbation in neuronal differentiation, synaptic plasticity and synapse and neural network formation. The *Pcdh9* mutation may exert synergistic effects via interactions with the Sin3A complex, as expression of the protocadherin gene cluster is regulated by CTCF recruitment of TET demethylases to the Sin3A complex for *Pcdha* promoter demethylation[71]. Thus, the *Pcdha9* mutation may amplify impact of the *Sap130* mutation via perturbation of protocadherin regulated patterning of synaptic connectivity. This may account for the finding of similar neurobehavioral deficits in the Emx1-Cre:*Sap130*$^{f/-}$ mice with microcephaly, and *Pcdha9* mutant mice with largely normal brain anatomy. Interestingly, in Williams syndrome, a neurodevelopmental disorder associated with cognitive impairment and aortic valve defects, DNA hypermethylation of the *PCDHA* locus is also observed[72,73]. Our finding of behavioral impairment only in the female

Pcdha9$^{m/m}$ mice is unexplained, although Mecp2, a methyl-CPG binding protein causing Rett syndrome found in the Sin3A complex, is situated on the X-chromosome[74].

Transcriptome analysis of the *Ohia* mutant brain yielded similar neurodevelopmental/neurological disease pathways as those observed in the Emx1-Cre:*Sap130*$^{f/-}$mice, supporting the notion that *Sap130* and *Pcdha9* likely act on convergent pathways. Many of these diseases are known to be associated with HLHS, such as intellectual disability, impaired cognition, autism, and development disorders. As we observed the same disease pathways when the differentially expressed genes were intersected with genes recovered from the DNA methylation analysis and the ChiPseq analysis, this suggested the gene expression changes in the *Ohia* brain reflect transcriptional changes involving Sap130 modulated DNA methylation. Consistent with this, *Sap130* and *Sin3A* were previously shown to be required for R-loop formation, an abundant three stranded structure shown to promote transcription by blocking gene promoter DNA methylation[75,76]. The essential role of *Sap130* in orchestrating this epigenetic regulation is indicated by the observation that in the *Emx1-Cre:Sap130*$^{-/flx}$ mice*,* the microcephaly phenotype exhibited 100% penetrance as compared to the 30-50% penetrance in the *Ohia* mutant mice harboring a hypomorphic *Sap130* mutation. The recovery of DNA methylation" and "HOTAIR regulation" in transcriptome profiling of the *Emx1-Cre:Sap130*$^{-/flx}$ forebrain provided further support of the essential role of *Sap130* in regulating DNA methylation. The importance of DNA methylation in neurodevelopmental disorders is well documented by the recent identification of methylation signatures for 42 neurodevelopmental disorders, and also for schizophrenia, autism, bipolar disorder, and attention deficit hyperactivity disorder[30,77,78]. DNA methylation signature has also been recently reported for Witteveen-Kolk syndrome, further pointing to involvement of the Sin3A complex in such epigenetic regulation[79].

While our study is based on interrogating the only genetically defined mouse model of HLHS, the *Ohia* mutant, the fact that our mice exhibit phenotypes similar to those reported clinically for patients with HLHS would suggest there are convergent pathways underlying the

shared disease phenotypes regardless of their genetic etiology. This would suggest our findings will have broad relevance for insights into the disease mechanisms contributing to the poor neurodevelopment associated with HLHS. Our finding of an intrinsic spindle defect may explain the failure to improve neurocognitive outcome with in utero aortic valvuloplasty[21]. The therapeutic application of maternal hyperoxygenation in utero to promote brain growth also may be confounded by defects in neurovascular coupling that may impair brain oxygenation even in the setting of maternal hyperoxygenation[80,81]. However, treatment to elevate NO might have therapeutic potential if it can restore neurovascular coupling and also NO dependent CREB signaling. Epigenetic therapy also may be possible with drugs targeting DNA methylation or DNA methyltransferases[82]. We note an *Ohia* pig model is being generated, and with a gyrencephalic brain, it will be superior for modeling brain defects associated with HLHS, and testing the efficacy of new therapies to improve neurodevelopment in HLHS [83].

.

Author Contributions

GCG, BJG, MGS performed mouse husbandry and genotyping, GCG performed mouse brain immunostaining and cell culture work; GCG, AB, LH, HY performed RNAseq, ChIPseq, and methylation experiments and analysis; MG assisted with PPI visualization, GCG and DS performed mouse behavioral testing and analysis; GCG, WTR performed episcopic confocal microscopy analysis of mouse brains; XX performed human iPSC methylation analysis, MCS and YLW performed brain MRI imaging and analysis, GCG and CWL participated in the experimental design and analysis of results; GCG, BJG, AP, CWL performed manuscript writing and editing. All authors approved the final manuscript.

Sources of Funding

This research was supported by NIH grants HD097967 (GCG) and HL14278 (CWL). YLW is supported by funding from AHA (18CDA34140024), NIH (EB023507, NS121706), and DoD (W81XWH1810070).

Disclosures

The authors report no disclosures.

REFERENCES

1. Reller MD, Strickland MJ, Riehle-Colarusso T, Mahle WT and Correa A. Prevalence of congenital heart defects in metropolitan Atlanta, 1998-2005. *The Journal of pediatrics*. 2008;153:807-813.
2. Hoffman JI and Kaplan S. The incidence of congenital heart disease. *Journal of the American college of cardiology*. 2002;39:1890-1900.
3. Marino BS, Lipkin PH, Newburger JW, Peacock G, Gerdes M, Gaynor JW, Mussatto KA, Uzark K, Goldberg CS and Johnson Jr WH. Neurodevelopmental outcomes in children with congenital heart disease: evaluation and management: a scientific statement from the American Heart Association. *Circulation*. 2012;126:1143-1172.
4. Marelli A, Miller SP, Marino BS, Jefferson AL and Newburger JW. Brain in Congenital Heart Disease Across the Lifespan. *Circulation*. 2016;133:1951-1962.
5. Gaynor JW, Wernovsky G, Jarvik GP, Bernbaum J, Gerdes M, Zackai E, Nord AS, Clancy RR, Nicolson SC and Spray TL. Patient characteristics are important determinants of neurodevelopmental outcome at one year of age after neonatal and infant cardiac surgery. *The Journal of thoracic and cardiovascular surgery*. 2007;133:1344-1353. e3.
6. Fuller S, Nord AS, Gerdes M, Wernovsky G, Jarvik GP, Bernbaum J, Zackai E and Gaynor JW. Predictors of impaired neurodevelopmental outcomes at one year of age after infant cardiac surgery. *European journal of cardio-thoracic surgery*. 2009;36:40-48.
7. Newburger JW, Sleeper LA, Bellinger DC, Goldberg CS, Tabbutt S, Lu M, Mussatto KA, Williams IA, Gustafson KE and Mital S. Early developmental outcome in children with hypoplastic left heart syndrome and related anomalies: the single ventricle reconstruction trial. *Circulation*. 2012;125:2081-2091.
8. Hinton RB, Andelfinger G, Sekar P, Hinton AC, Gendron RL, Michelfelder EC, Robitaille Y and Benson DW. Prenatal head growth and white matter injury in hypoplastic left heart syndrome. *Pediatric research*. 2008;64:364-369.
9. Miller SP, McQuillen PS, Hamrick S, Xu D, Glidden DV, Charlton N, Karl T, Azakie A, Ferriero DM and Barkovich AJ. Abnormal brain development in newborns with congenital heart disease. *New England Journal of Medicine*. 2007;357:1928-1938.
10. Owen M, Shevell M, Majnemer A and Limperopoulos C. Abnormal brain structure and function in newborns with complex congenital heart defects before open heart surgery: a review of the evidence. *Journal of Child Neurology*. 2011;26:743-755.
11. Glauser TA, Rorke LB, Weinberg PM and Clancy RR. Congenital brain anomalies associated with the hypoplastic left heart syndrome. *Pediatrics*. 1990;85:984-990.
12. Homsy J, Zaidi S, Shen Y, Ware JS, Samocha KE, Karczewski KJ, DePalma SR, McKean D, Wakimoto H and Gorham J. De novo mutations in congenital heart disease with neurodevelopmental and other congenital anomalies. *Science*. 2015;350:1262-1266.
13. Zaidi S, Choi M, Wakimoto H, Ma L, Jiang J, Overton JD, Romano-Adesman A, Bjornson RD, Breitbart RE and Brown KK. De novo mutations in histone-modifying genes in congenital heart disease. *Nature*. 2013;498:220-223.
14. Schanen NC. Epigenetics of autism spectrum disorders. *Human molecular genetics*. 2006;15:R138-R150.

15. Bucholz EM, Sleeper LA, Goldberg CS, Pasquali SK, Anderson BR, Gaynor JW, Cnota JF and Newburger JW. Socioeconomic Status and Long-term Outcomes in Single Ventricle Heart Disease. *Pediatrics*. 2020;146.
16. Rollins CK, Newburger JW and Roberts AE. Genetic contribution to neurodevelopmental outcomes in congenital heart disease: are some patients predetermined to have developmental delay? *Curr Opin Pediatr*. 2017;29:529-533.
17. Goldberg CS, Hu C, Brosig C, Gaynor JW, Mahle WT, Miller T, Mussatto KA, Sananes R, Uzark K, Trachtenberg F, Pizarro C, Pemberton VL, Lewis AB, Li JS, Jacobs JP, Cnota J, Atz AM, Lai WW, Bellinger D, Newburger JW and Phn I. Behavior and Quality of Life at 6 Years for Children With Hypoplastic Left Heart Syndrome. *Pediatrics*. 2019;144.
18. Sananes R, Goldberg CS, Newburger JW, Hu C, Trachtenberg F, Gaynor JW, Mahle WT, Miller T, Uzark K, Mussatto KA, Pizarro C, Jacobs JP, Cnota J, Atz AM, Lai WW, Burns KM, Milazzo A, Votava-Smith J, Brosig CL and investigators PHN. Six-Year Neurodevelopmental Outcomes for Children With Single-Ventricle Physiology. *Pediatrics*. 2021;147.
19. Siciliano RE, Prussien KV, Lee CA, Patel NJ, Murphy LK, Compas BE and Jordan LC. Cognitive Function in Pediatric Hypoplastic Left Heart Syndrome: Systematic Review and Meta-Analysis. *J Pediatr Psychol*. 2019;44:937-947.
20. Hangge PT, Cnota JF, Woo JG, Hinton AC, Divanovic AA, Manning PB, Ittenbach RF and Hinton RB. Microcephaly is associated with early adverse neurologic outcomes in hypoplastic left heart syndrome. *Pediatr Res*. 2013;74:61-7.
21. Laraja K, Sadhwani A, Tworetzky W, Marshall AC, Gauvreau K, Freud L, Hass C, Dunbar-Masterson C, Ware J, Lafranchi T, Wilkins-Haug L and Newburger JW. Neurodevelopmental Outcome in Children after Fetal Cardiac Intervention for Aortic Stenosis with Evolving Hypoplastic Left Heart Syndrome. *J Pediatr*. 2017;184:130-136 e4.
22. Liu X, Yagi H, Saeed S, Bais AS, Gabriel GC, Chen Z, Peterson KA, Li Y, Schwartz MC and Reynolds WT. The complex genetics of hypoplastic left heart syndrome. *Nature genetics*. 2017;49:1152-1159.
23. Witteveen JS, Willemsen MH, Dombroski TC, Van Bakel NH, Nillesen WM, Van Hulten JA, Jansen EJ, Verkaik D, Veenstra-Knol HE and van Ravenswaaij-Arts CM. Haploinsufficiency of MeCP2-interacting transcriptional co-repressor SIN3A causes mild intellectual disability by affecting the development of cortical integrity. *Nature Genetics*. 2016;48:877-887.
24. Amir RE, Van den Veyver IB, Wan M, Tran CQ, Francke U and Zoghbi HY. Rett syndrome is caused by mutations in X-linked MECP2, encoding methyl-CpG-binding protein 2. *Nat Genet*. 1999;23:185-8.
25. Thu CA, Chen WV, Rubinstein R, Chevee M, Wolcott HN, Felsovalyi KO, Tapia JC, Shapiro L, Honig B and Maniatis T. Single-cell identity generated by combinatorial homophilic interactions between α, β, and γ protocadherins. *Cell*. 2014;158:1045-1059.
26. Mountoufaris G, Chen WV, Hirabayashi Y, O'Keeffe S, Chevee M, Nwakeze CL, Polleux F and Maniatis T. Multicluster Pcdh diversity is required for mouse olfactory neural circuit assembly. *Science*. 2017;356:411-414.
27. Anitha A, Thanseem I, Nakamura K, Yamada K, Iwayama Y, Toyota T, Iwata Y, Suzuki K, Sugiyama T and Tsujii M. Protocadherin α (PCDHA) as a novel susceptibility gene for autism. *Journal of Psychiatry and Neuroscience*. 2013;38:192-198.

28. Zhu F, Zhu Q, Ye D, Zhang Q, Yang Y, Guo X, Liu Z, Jiapaer Z, Wan X, Wang G, Chen W, Zhu S, Jiang C, Shi W and Kang J. Sin3a-Tet1 interaction activates gene transcription and is required for embryonic stem cell pluripotency. *Nucleic Acids Res*. 2018;46:6026-6040.
29. Shirvani-Farsani Z, Maloum Z, Bagheri-Hosseinabadi Z, Vilor-Tejedor N and Sadeghi I. DNA methylation signature as a biomarker of major neuropsychiatric disorders. *Journal of Psychiatric Research*. 2021;141:34-49.
30. Aref-Eshghi E, Kerkhof J, Pedro VP, Groupe DIF, Barat-Houari M, Ruiz-Pallares N, Andrau JC, Lacombe D, Van-Gils J, Fergelot P, Dubourg C, Cormier-Daire V, Rondeau S, Lecoquierre F, Saugier-Veber P, Nicolas G, Lesca G, Chatron N, Sanlaville D, Vitobello A, Faivre L, Thauvin-Robinet C, Laumonnier F, Raynaud M, Alders M, Mannens M, Henneman P, Hennekam RC, Velasco G, Francastel C, Ulveling D, Ciolfi A, Pizzi S, Tartaglia M, Heide S, Heron D, Mignot C, Keren B, Whalen S, Afenjar A, Bienvenu T, Campeau PM, Rousseau J, Levy MA, Brick L, Kozenko M, Balci TB, Siu VM, Stuart A, Kadour M, Masters J, Takano K, Kleefstra T, de Leeuw N, Field M, Shaw M, Gecz J, Ainsworth PJ, Lin H, Rodenhiser DI, Friez MJ, Tedder M, Lee JA, DuPont BR, Stevenson RE, Skinner SA, Schwartz CE, Genevieve D and Sadikovic B. Evaluation of DNA Methylation Episignatures for Diagnosis and Phenotype Correlations in 42 Mendelian Neurodevelopmental Disorders. *Am J Hum Genet*. 2020;106:356-370.
31. Xu X, Jin K, Bais AS, Zhu W, Yagi H, Feinstein TN, Nguyen PK, Criscione JD, Liu X, Beutner G, Karunakaran KB, Rao KS, He H, Adams P, Kuo CK, Kostka D, Pryhuber GS, Shiva S, Ganapathiraju MK, Porter GA, Lin J-HI, Aronow B and Lo CW. Uncompensated mitochondrial oxidative stress underlies heart failure in an iPSC-derived model of congenital heart disease. *Cell Stem Cell*. 2022.
32. Nicholas AK, Swanson EA, Cox JJ, Karbani G, Malik S, Springell K, Hampshire D, Ahmed M, Bond J and Di Benedetto D. The molecular landscape of ASPM mutations in primary microcephaly. *Journal of medical genetics*. 2009;46:249-253.
33. Nicholas AK, Khurshid M, Désir J, Carvalho OP, Cox JJ, Thornton G, Kausar R, Ansar M, Ahmad W and Verloes A. WDR62 is associated with the spindle pole and is mutated in human microcephaly. *Nature genetics*. 2010;42:1010-1014.
34. Rodenas-Ruano A, Chávez AE, Cossio MJ, Castillo PE and Zukin RS. REST-dependent epigenetic remodeling promotes the developmental switch in synaptic NMDA receptors. *Nature neuroscience*. 2012;15:1382-1390.
35. Bray NJ, Preece A, Williams NM, Moskvina V, Buckland PR, Owen MJ and O'Donovan MC. Haplotypes at the dystrobrevin binding protein 1 (DTNBP1) gene locus mediate risk for schizophrenia through reduced DTNBP1 expression. *Human molecular genetics*. 2005;14:1947-1954.
36. Lang F, Strutz‐Seebohm N, Seebohm G and Lang UE. Significance of SGK1 in the regulation of neuronal function. *The Journal of physiology*. 2010;588:3349-3354.
37. Ma YL, Tsai MC, Hsu WL and Lee EH. SGK protein kinase facilitates the expression of long-term potentiation in hippocampal neurons. *Learn Mem*. 2006;13:114-8.
38. Saura CA and Valero J. The role of CREB signaling in Alzheimer's disease and other cognitive disorders. *Rev Neurosci*. 2011;22:153-69.
39. Gau D, Lemberger T, von Gall C, Kretz O, Le Minh N, Gass P, Schmid W, Schibler U, Korf HW and Schutz G. Phosphorylation of CREB Ser142 regulates light-induced phase shifts of the circadian clock. *Neuron*. 2002;34:245-53.

40. Stackhouse TL and Mishra A. Neurovascular Coupling in Development and Disease: Focus on Astrocytes. *Front Cell Dev Biol*. 2021;9:702832.
41. Donofrio M, Bremer Y, Schieken R, Gennings C, Morton L, Eidem B, Cetta F, Falkensammer C, Huhta J and Kleinman C. Autoregulation of cerebral blood flow in fetuses with congenital heart disease: the brain sparing effect. *Pediatric cardiology*. 2003;24:436-443.
42. Kinnear C, Haranal M, Shannon P, Jaeggi E, Chitayat D and Mital S. Abnormal fetal cerebral and vascular development in hypoplastic left heart syndrome. *Prenat Diagn*. 2019;39:38-44.
43. Riccio A, Alvania RS, Lonze BE, Ramanan N, Kim T, Huang Y, Dawson TM, Snyder SH and Ginty DD. A nitric oxide signaling pathway controls CREB-mediated gene expression in neurons. *Mol Cell*. 2006;21:283-94.
44. Jiang J, Chan Y-S, Loh Y-H, Cai J, Tong G-Q, Lim C-A, Robson P, Zhong S and Ng H-H. A core Klf circuitry regulates self-renewal of embryonic stem cells. *Nature cell biology*. 2008;10:353-360.
45. Lavallée G, Andelfinger G, Nadeau M, Lefebvre C, Nemer G, Horb ME and Nemer M. The Kruppel ‐ like transcription factor KLF13 is a novel regulator of heart development. *The EMBO journal*. 2006;25:5201-5213.
46. Ávila-Mendoza J, Subramani A and Denver RJ. Krüppel-like factors 9 and 13 block axon growth by transcriptional repression of key components of the cAMP signaling pathway. *Frontiers in Molecular Neuroscience*. 2020:217.
47. Williams K, Christensen J, Pedersen MT, Johansen JV, Cloos PA, Rappsilber J and Helin K. TET1 and hydroxymethylcytosine in transcription and DNA methylation fidelity. *Nature*. 2011;473:343-348.
48. Bhat V, Girimaji SC, Mohan G, Arvinda HR, Singhmar P, Duvvari MR and Kumar A. Mutations in WDR62, encoding a centrosomal and nuclear protein, in Indian primary microcephaly families with cortical malformations. *Clin Genet*. 2011;80:532-40.
49. Gorski JA, Talley T, Qiu M, Puelles L, Rubenstein JL and Jones KR. Cortical excitatory neurons and glia, but not GABAergic neurons, are produced in the Emx1-expressing lineage. *Journal of Neuroscience*. 2002;22:6309-6314.
50. Zhang Y, Tian Y, Yu J-J, He J, Luo J, Zhang S, Tang C-E and Tao Y-m. Overexpression of WDR62 is associated with centrosome amplification in human ovarian cancer. *Journal of ovarian research*. 2013;6:1-6.
51. Sadhwani A, Wypij D, Rofeberg V, Gholipour A, Mittleman M, Rohde J, Velasco-Annis C, Calderon J, Friedman KG, Tworetzky W, Grant PE, Soul JS, Warfield SK, Newburger JW, Ortinau CM and Rollins CK. Fetal Brain Volume Predicts Neurodevelopment in Congenital Heart Disease. *Circulation*. 2022;145:1108-1119.
52. Limperopoulos C, Tworetzky W, McElhinney DB, Newburger JW, Brown DW, Robertson RL, Jr., Guizard N, McGrath E, Geva J, Annese D, Dunbar-Masterson C, Trainor B, Laussen PC and du Plessis AJ. Brain volume and metabolism in fetuses with congenital heart disease: evaluation with quantitative magnetic resonance imaging and spectroscopy. *Circulation*. 2010;121:26-33.
53. Sun L, Macgowan CK, Sled JG, Yoo SJ, Manlhiot C, Porayette P, Grosse-Wortmann L, Jaeggi E, McCrindle BW, Kingdom J, Hickey E, Miller S and Seed M. Reduced fetal cerebral oxygen consumption is associated with smaller brain size in fetuses with congenital heart disease. *Circulation*. 2015;131:1313-23.
54. Adams PS, Zahid M, Khalifa O, Feingold B and Lo CW. Low Nasal NO in Congenital Heart Disease With Systemic Right Ventricle and Postcardiac Transplantation. *J Am Heart Assoc*. 2017;6.

55. Schmithorst VJ, Adams PS, Badaly D, Lee VK, Wallace J, Beluk N, Votava-Smith JK, Weinberg JG, Beers SR, Detterich J, Wood JC, Lo CW and Panigrahy A. Impaired Neurovascular Function Underlies Poor Neurocognitive Outcomes and Is Associated with Nitric Oxide Bioavailability in Congenital Heart Disease. *Metabolites*. 2022;12.
56. Rollins CK, Ortinau CM, Stopp C, Friedman KG, Tworetzky W, Gagoski B, Velasco-Annis C, Afacan O, Vasung L, Beaute JI, Rofeberg V, Estroff JA, Grant PE, Soul JS, Yang E, Wypij D, Gholipour A, Warfield SK and Newburger JW. Regional Brain Growth Trajectories in Fetuses with Congenital Heart Disease. *Ann Neurol*. 2021;89:143-157.
57. Qureshi IA, Gokhan S and Mehler MF. REST and CoREST are transcriptional and epigenetic regulators of seminal neural fate decisions. *Cell Cycle*. 2010;9:4477-86.
58. Ballas N, Grunseich C, Lu DD, Speh JC and Mandel G. REST and its corepressors mediate plasticity of neuronal gene chromatin throughout neurogenesis. *Cell*. 2005;121:645-657.
59. Gao Z, Ure K, Ding P, Nashaat M, Yuan L, Ma J, Hammer RE and Hsieh J. The master negative regulator REST/NRSF controls adult neurogenesis by restraining the neurogenic program in quiescent stem cells. *Journal of Neuroscience*. 2011;31:9772-9786.
60. Huang Y, Myers SJ and Dingledine R. Transcriptional repression by REST: recruitment of Sin3A and histone deacetylase to neuronal genes. *Nature neuroscience*. 1999;2:867-872.
61. Tang T, Zhang Y, Wang Y, Cai Z, Lu Z, Li L, Huang R, Hagelkruys A, Matthias P and Zhang H. HDAC1 and HDAC2 regulate intermediate progenitor positioning to safeguard neocortical development. *Neuron*. 2019;101:1117-1133. e5.
62. Yang YJ, Baltus AE, Mathew RS, Murphy EA, Evrony GD, Gonzalez DM, Wang EP, Marshall-Walker CA, Barry BJ and Murn J. Microcephaly gene links trithorax and REST/NRSF to control neural stem cell proliferation and differentiation. *Cell*. 2012;151:1097-1112.
63. Chen J-F, Zhang Y, Wilde J, Hansen KC, Lai F and Niswander L. Microcephaly disease gene Wdr62 regulates mitotic progression of embryonic neural stem cells and brain size. *Nature communications*. 2014;5:1-13.
64. Marthiens V, Rujano MA, Pennetier C, Tessier S, Paul-Gilloteaux P and Basto R. Centrosome amplification causes microcephaly. *Nature cell biology*. 2013;15:731-740.
65. Guo J, Otis JM, Higginbotham H, Monckton C, Cheng J, Asokan A, Mykytyn K, Caspary T, Stuber GD and Anton ES. Primary Cilia Signaling Shapes the Development of Interneuronal Connectivity. *Dev Cell*. 2017;42:286-300 e4.
66. Nanni L, Ming JE, Bocian M, Steinhaus K, Bianchi DW, de Die-Smulders C, Giannotti A, Imaizumi K, Jones KL, Del Campo M, Martin RA, Meinecke P, Pierpont MEM, Robin NH, Young ID, Roessler E and Muenke M. The Mutational Spectrum of the Sonic Hedgehog Gene in Holoprosencephaly: SHH Mutations Cause a Significant Proportion of Autosomal Dominant Holoprosencephaly. *Human Molecular Genetics*. 1999;8:2479-2488.
67. Koefoed K, Veland IR, Pedersen LB, Larsen LA and Christensen ST. Cilia and coordination of signaling networks during heart development. *Organogenesis*. 2014;10:108-125.
68. Geddes GC, Stamm K, Mitchell M, Mussatto KA and Tomita-Mitchell A. Ciliopathy variant burden and developmental delay in children with hypoplastic left heart syndrome. *Genetics in Medicine*. 2017;19:711-714.
69. Bagge CN, Henderson VW, Laursen HB, Adelborg K, Olsen M and Madsen NL. Risk of Dementia in Adults With Congenital Heart Disease: Population-Based Cohort Study. *Circulation*. 2018;137:1912-1920.

70. Servili E, Trus M, Sajman J, Sherman E and Atlas D. Elevated basal transcription can underlie timothy channel association with autism related disorders. *Prog Neurobiol*. 2020;191:101820.
71. Canzio D, Nwakeze CL, Horta A, Rajkumar SM, Coffey EL, Duffy EE, Duffié R, Monahan K, o'Keeffe S and Simon MD. Antisense lncRNA transcription mediates DNA demethylation to drive stochastic protocadherin α promoter choice. *Cell*. 2019;177:639-653. e15.
72. El Hajj N, Dittrich M and Haaf T. Epigenetic dysregulation of protocadherins in human disease. *Seminars in cell & developmental biology*. 2017;69:172-182.
73. Strong E, Butcher DT, Singhania R, Mervis CB, Morris CA, De Carvalho D, Weksberg R and Osborne LR. Symmetrical dose-dependent DNA-methylation profiles in children with deletion or duplication of 7q11. 23. *The American Journal of Human Genetics*. 2015;97:216-227.
74. Amir RE, Van den Veyver IB, Wan M, Tran CQ, Francke U and Zoghbi HY. Rett syndrome is caused by mutations in X-linked MECP2, encoding methyl-CpG-binding protein 2. *Nature genetics*. 1999;23:185-188.
75. Salas-Armenteros I, Perez-Calero C, Bayona-Feliu A, Tumini E, Luna R and Aguilera A. Human THO-Sin3A interaction reveals new mechanisms to prevent R-loops that cause genome instability. *EMBO J*. 2017;36:3532-3547.
76. Grunseich C, Wang IX, Watts JA, Burdick JT, Guber RD, Zhu Z, Bruzel A, Lanman T, Chen K, Schindler AB, Edwards N, Ray-Chaudhury A, Yao J, Lehky T, Piszczek G, Crain B, Fischbeck KH and Cheung VG. Senataxin Mutation Reveals How R-Loops Promote Transcription by Blocking DNA Methylation at Gene Promoters. *Mol Cell*. 2018;69:426-437 e7.
77. Chater-Diehl E, Goodman SJ, Cytrynbaum C, Turinsky AL, Choufani S and Weksberg R. Anatomy of DNA methylation signatures: Emerging insights and applications. *Am J Hum Genet*. 2021;108:1359-1366.
78. Shirvani-Farsani Z, Maloum Z, Bagheri-Hosseinabadi Z, Vilor-Tejedor N and Sadeghi I. DNA methylation signature as a biomarker of major neuropsychiatric disorders. *J Psychiatr Res*. 2021;141:34-49.
79. Coenen-van der Spek J, Relator R, Kerkhof J, McConkey H, Levy MA, Tedder ML, Louie RJ, Fletcher RS, Moore HW, Childers A, Farrelly ER, Champaigne NL, Lyons MJ, Everman DB, Rogers RC, Skinner SA, Renck A, Matalon DR, Dills SK, Monteleone B, Demirdas S, Dingemans AJM, Donker Kaat L, Kolk SM, Pfundt R, Rump P, Sadikovic B, Kleefstra T and Butler KM. DNA methylation episignature for Witteveen-Kolk syndrome due to SIN3A haploinsufficiency. *Genet Med*. 2023;25:63-75.
80. Co-Vu J, Lopez-Colon D, Vyas HV, Weiner N and DeGroff C. Maternal hyperoxygenation: A potential therapy for congenital heart disease in the fetuses? A systematic review of the current literature. *Echocardiography*. 2017;34:1822-1833.
81. Edwards LA, Lara DA, Sanz Cortes M, Hunter JV, Andreas S, Nguyen MJ, Schoppe LJ, Zhang J, Smith EM, Maskatia SA, Sexson-Tejtel SK, Lopez KN, Lawrence EJ, Wang Y, Challman M, Ayres NA, Altman CA, Aagaard K, Becker JA and Morris SA. Chronic Maternal Hyperoxygenation and Effect on Cerebral and Placental Vasoregulation and Neurodevelopment in Fetuses with Left Heart Hypoplasia. *Fetal Diagn Ther*. 2019;46:45-57.
82. Hu C, Liu X, Zeng Y, Liu J and Wu F. DNA methyltransferase inhibitors combination therapy for the treatment of solid tumor: mechanism and clinical application. *Clin Epigenetics*. 2021;13:166.

83. Gabriel GC, Devine W, Redel BK, Whitworth KM, Samuel M, Spate LD, Cecil RF, Prather RS, Wu Y and Wells KD. Cardiovascular Development and Congenital Heart Disease Modeling in the Pig. *Journal of the American Heart Association*. 2021;10:e021631.

Figure Legends

Figure 1. *Ohia*$^{m/m}$ mice display microcephaly with brain abnormalities.

A-D. E16.5 wildtype (A) and *Ohia*$^{m/m}$ mutant mouse brains exhibiting moderate (B) and severe (C) forebrain hypoplasia, with the severe mutant also showing holoprosencephaly. The distribution of brain phenotype severity in *Ohia*$^{m/m}$ mice is shown in the pie chart (D).

E-J. Episcopic confocal imaging of the head shown in the sagittal and coronal plane of a wildtype (+/+) (E,H) and two *Ohia*$^{m/m}$ mice, one with mild (B,F) and the other with severe (G,J) forebrain hypoplasia. Note hypoplastic (F) or absent (G) olfactory bulb, thin cortex (F,G), hypoplastic corpus callosum (I), and holoprosencephaly (J).

K-N. Cresyl violet stained sections from control (K), and two *Ohia* mutants with mild (L) vs. severe (M) forebrain hypoplasia. Quantification of 5 *Ohia* mutants and 5 littermate controls showed reduced cortical thickness (N). p=0.003, 2-tailed unpaired t-test.

Cx, cortex; OB, olfactory bulb; Cb, cerebellum; CC, corpus callosum; Lat V, lateral ventricle; Holo, holoprosencephaly. Scale bars = 0.5mm.

Figure 2. Impaired Cortical Plate Formation with Loss of Tbr2+ Intermediate Progenitors in *Ohia*$^{m/m}$ Mutant Brain

A-L. Sections of the brain of E16.5 control (A-D) and *Ohia*$^{m/m}$ mutant mice with mild (E-H) or severe (I-L) forebrain hypoplasia were stained with cresyl violet (A,E,I) to delineate the brain tissue architecture. Antibody staining was conducted for markers of apical progenitor cells (Pax6, B,F,J), intermediate progenitor cells (Tbr2 in C,G,K), and merged image showing both markers (D,H,L).

M-T. Section of the cortical plate of E16.5 wildtype (M-P) and mutant (Q-T) mouse brain was stained with antibodies to Satb2, marker for cortical layers II-IV (M,Q), Ctip2 for cortical layers V-VI (N,R), and Tbr1 (O,S) for cortical layer VI, and merged image showing all three markers (P,T).

U-Y. Quantification of number of cells stained by Pax6 (U), Tbr2 (V), Ctip2 (W), Tbr1 (X), and Satb2 (Y) in the brain of 5 *Ohia*$^{m/m}$ mutant and 5 littermate controls. P-values calculated by 2-tailed, unpaired t-test.

Scale bars in A-L indicate 500μm. Scale bars in M-T indicate 100μm.

Figure 3. Neural Progenitors in the Cortical Plate Show Mitotic Block With Increase in Cell Death and Possible Role for Multipolar Spindles Indicated by MEF Analysis

A-H. Comparison of the cortex of the brain from E14.5 *Ohia*$^{m/m}$ mutant (D-F) vs. wildtype littermate control embryos (A-C) showed more pH3 and TUNEL staining (G) in the ventricular (VZ) and

subventricular (SVC) zones in the mutants. A decrease was also noted in the proportion of mitotic cells in anaphase-telophase (H). P-value obtained using 2-way, unpaired t-test (n=3, *Ohia*$^{m/m}$ mutants, n=3 littermate controls).

I-N. MEFs generated from wildtype (I-K) and *Ohia*$^{m/m}$ mutant embryos (L-N) were immunostained with α-tubulin and γ-tubulin. Mitotic cells in the mutant MEFs showed increase in multipolar spindles (quantification in panel O). MEFs were generated from 3 *Ohia*$^{m/m}$ and 3 littermate control embryos, with >500 cells analyzed per embryo derived MEF. P-value calculated by 2-way, unpaired t-test.

P-R. *Ohia*$^{m/m}$ MEFs showed reduction in the proportion of mitotic cells in anaphase/telophase (P) and an increase in lagging chromosomes during anaphase (Q,R) P-value obtained using 2-way, unpaired t-test.

CP, cortical plate; IZ, intermediate zone; SVZ, subventricular zone; VZ, ventricular zone; P/M, prophase/metaphase; A/T, anaphase/telophase. Scale bars = 100µm.

Figure 4. Transcriptome Profiling Shows Dysregulated Neurodevelopment in *Ohia*$^{m/m}$ Mutants

Differentially expressed genes (DEGs) recovered from RNAseq analysis of E14.5 *Ohia* mutant brain were analyzed for pathway enrichment using Metascape (A), Ingenuity Pathway Analysis (IPA) for upstream regulators of downstream neurodevelopmental outcomes (B, red for upregulated, green for downregulated), IPA canonical pathway (C), and IPA curated CREB signaling pathway (D), with purple outline indicating genes found to be differentially expressed, with green fill for downregulated and red fill for upregulated DEGs. (E) Disease terms recovered from ToppGene analysis of recovered DEGs.

Figure 5. Dysregulated Expression of Genes Associated with Neurovascular Coupling. Modified IPA curated neurovascular coupling pathway illustrating dysregulated expression of genes involved in neurovascular coupling. DEGs identified in *Ohia* brain highlighted in purple outline.

Figure 6. Sap130 Chromatin Immunoprecipitation Sequencing Analysis of Mouse Brain and Examination of Cilia in the *Ohia* Brain Tissue

ChIP-seq analysis of wildtype E14.5 mouse embryo brain was conducted using Sap130 antibody.

A. Sap130 occupancy in the 5' upstream promoter region of selected genes is shown in panel A, including Rest and Sin3A, and two genes associated with microcephaly (*Aspm, Wdr62*).

B-E. Pathways in GO Biological Process (B) and Cellular Components (C), as well as Human Phenotype (D), and Disease (E) terms recovered from ToppGene gene enrichment analysis of Sap130 ChIPseq target genes.

F. Motif enrichment analysis of the Sap130 ChIPseq target genes identified putative Sap130 DNA binding sequences.

G-I. Cilia visualization in sections of wildtype (G) and *Ohia*$^{m/m}$ mutant brain tissue (H) immunostained with Arl13b (cilia, green), γ-tub (centrosome, red) and DAPI. Quantification showed reduction of cilia in the mutant brain (I, n=3 *Ohia* mutant and 4 littermate controls). P value determined by 2-tailed, unpaired t-test.

Figure 7. Molecular profiling of *Ohia*$^{m/m}$ brain tissue with integration of genome-wide methylome with RNAseq and Sap130 ChIPseq analyses.

A. Quantification of methyl-CpGs in promoter region of wildtype (n=3, C1, C2, C3) and *Ohia*$^{m/m}$ brain (n=3, S1, S2, S3) tissue revealed reduced DNA methylation in the *Ohia*$^{m/m}$ brain tissue.

B,C. Antibody staining for mCpG in iPSC cardiomyocytes showed less staining in the HLHS patient vs. control iPSC-CM (B). This was confirmed with quantification shown in scatter plot (mean±SEM) for n=200 cells from two control subjects and n=409 cells from four HLHS subjects (C). P-value determined by Mann-Whitney test.

D. Increased methylation of two CpG sites in two DMRS found in *Klf17* (denoted by red asterisk) in the *Ohia*$^{m/m}$ brain tissue.

E,F. Venn diagrams show two-way intersection of downregulated DEGs with genes associated with DMR (E) and three-way intersection of down regulated DEGs, genes associated with DMR, and genes recovered from Sap130 ChiPseq (F).

G, H. ToppGene enrichment analysis for Mouse Phenotypes recovered from the two-way (G) or three-way (H) intersection of the downregulated DEGS with genes associated with DMRs or with DMRs and Sap130 ChIP target genes.

I. Circle plot showing significant Disease association identified by the ToppGene enrichment analysis of the RNAseq recovered down regulated DEGs (first column), genes shared between the down regulated DEGs and DMR associated genes (second column) and the down regulated DEGs, DMR associated genes, and ChIPseq target genes (third column). All three analyses yielded the same Diseases, but with somewhat different p-value ranking as shown by the color coding in the circle plot.

Figure 8. *Emx1-cre Sap130$^{f/-}$* Mice Show Microcephaly With Transcriptome Profiling Showing Abnormal Neurodevelopment

A. Wildtype newborn control (left) and *Emx1-cre Sap130$^{f/-}$* mutant (right) brains.

Scale bar = 500µm.

B. Brain/body weight ratio for newborn control and *Emx1-cre Sap130$^{f/-}$* mice confirm brain hypoplasia in the *Emx1-cre Sap130$^{f/-}$* mice.

C. qPCR of *Sap130* transcripts in E14.5 forebrain tissue from 4 control and 4 *Emx1-cre Sap130$^{f/-}$* mice showed decrease in *Sap130* transcripts, demonstrating efficacy of the Emx1-Cre mediated *Sap130* deletion.

D. qPCR of *Wdr62* transcripts in E14.5 forebrain tissue from 4 control and 4 *Emx1-cre Sap130$^{f/-}$* mice showed increased transcript expression, indicating possible centrosome amplification.

E-I. IPA and ToppGene analysis of DEGs from RNAseq of E14.5 forebrain tissue from *Emx1-cre Sap130$^{f/-}$* vs. control mice. Shown are the results obtained with IPA Canonical Pathway (E), IPA Gene Set (G) for hallmark centrosome, hypoxia, and mitotic spindle genes, and ToppGene analysis for Disease (H) and Mouse Phenotype (I).

Figure 9. Brain and Behavioral Analysis of *Emx1-cre Sap130$^{f/-}$* and *Pcdha9$^{m/m}$* Adult Mice

A-F. Adult brain MRI of wildtype (A), and *Emx1-cre;Sap130$^{f/-}$* adult mice (B). Note the marked reduction in size of the cortex. Quantitative analysis showed significant reduction in brain volumes associated with the corpus callous (C), the cerebral cortex (D), the hippocampus (E), and forebrain (F).

G,H. Adult brain MRI of wildtype (A), and *Pcdha9$^{m/m}$* adult mice (B). No change was observed in anatomical structure of the *Pcdha9$^{m/m}$* mouse brain.

I-N. Neurobehavioral testing was conducted using three tests: Morris water maze (I,J), cued fear conditioning (K,L), and three chamber sociability test (M,N). In both *Pcdha9$^{m/m}$* female mice and *Emx1-cre:Sap130$^{f/-}$* mice, significant deficits were observed for fear conditioning and sociability, but no difference was observed in the Morris water maze. Similar analysis of *Pcdha9$^{m/m}$* male mice showed no change relative to wildtype control male mice (Supplemental Figure S7). Morris water maze analyzed by 2-way repeated measures ANOVA, fear conditioning analyzed by 2-way repeated measures ANOVA, and sociability tested analyzed by two-way and three-way ANOVA.

Figures

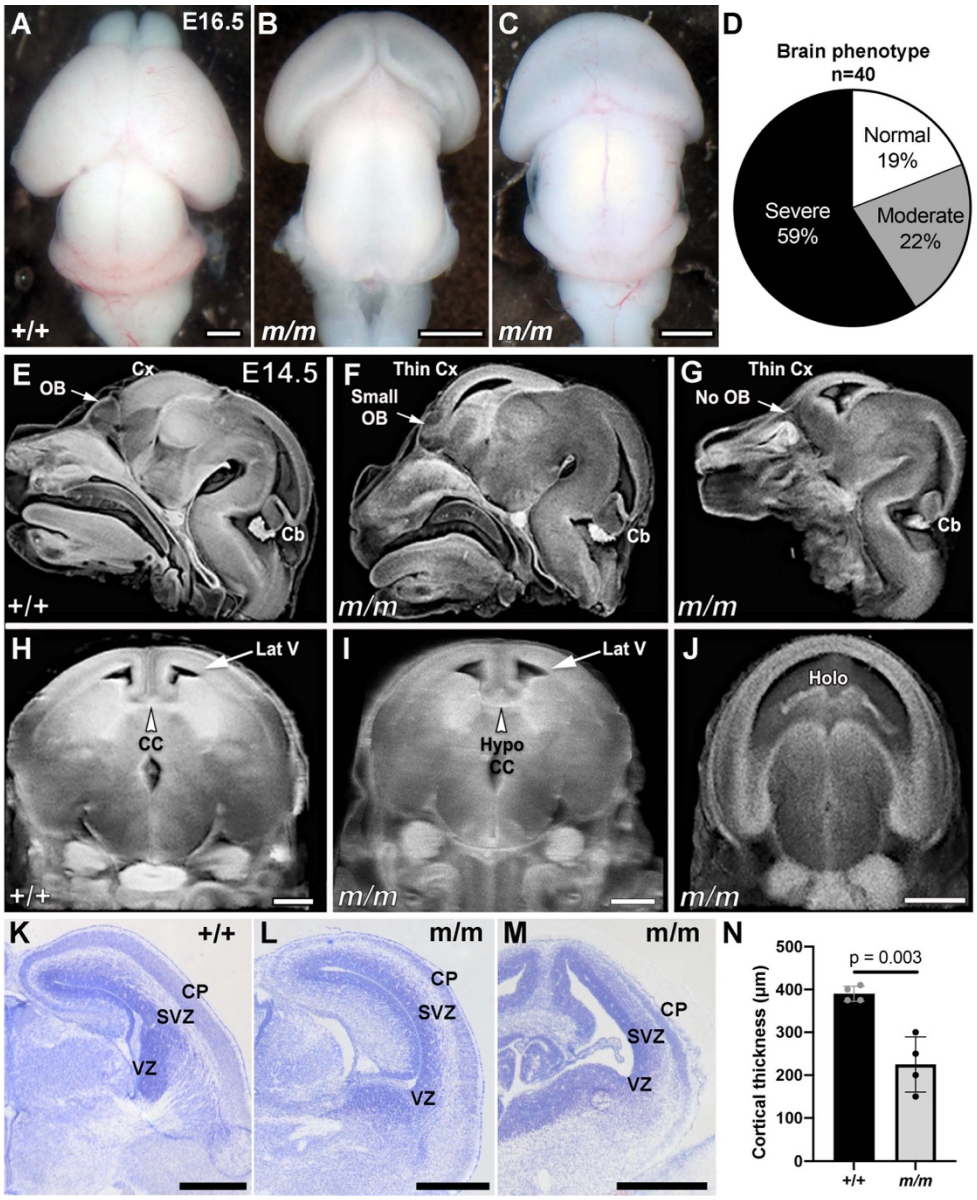

Figure 1. *Ohia*$^{m/m}$ mice display microcephaly with brain abnormalities.

A-D. E16.5 wildtype (A) and *Ohia*$^{m/m}$ mutant mouse brains exhibiting moderate (B) and severe (C) forebrain hypoplasia, with the severe mutant also showing holoprosencephaly. The distribution of brain phenotype severity in *Ohia*$^{m/m}$ mice is shown in the pie chart (D).

E-J. Episcopic confocal imaging of the head shown in the sagittal and coronal plane of a wildtype (+/+) (E,H) and two *Ohia*$^{m/m}$ mice, one with mild (B,F) and the other with severe (G,J) forebrain hypoplasia. Note hypoplastic (F) or absent (G) olfactory bulb, thin cortex (F,G), hypoplastic corpus callosum (I), and holoprosencephaly (J).

K-N. Cresyl violet stained sections from control (K), and two *Ohia* mutants with mild (L) vs. severe (M) forebrain hypoplasia. Quantification of 5 *Ohia* mutants and 5 littermate controls showed reduced cortical thickness (N). p=0.003, 2-tailed unpaired t-test.

Cx, cortex; OB, olfactory bulb; Cb, cerebellum; CC, corpus callosum; Lat V, lateral ventricle; Holo, holoprosencephaly. Scale bars = 0.5mm.

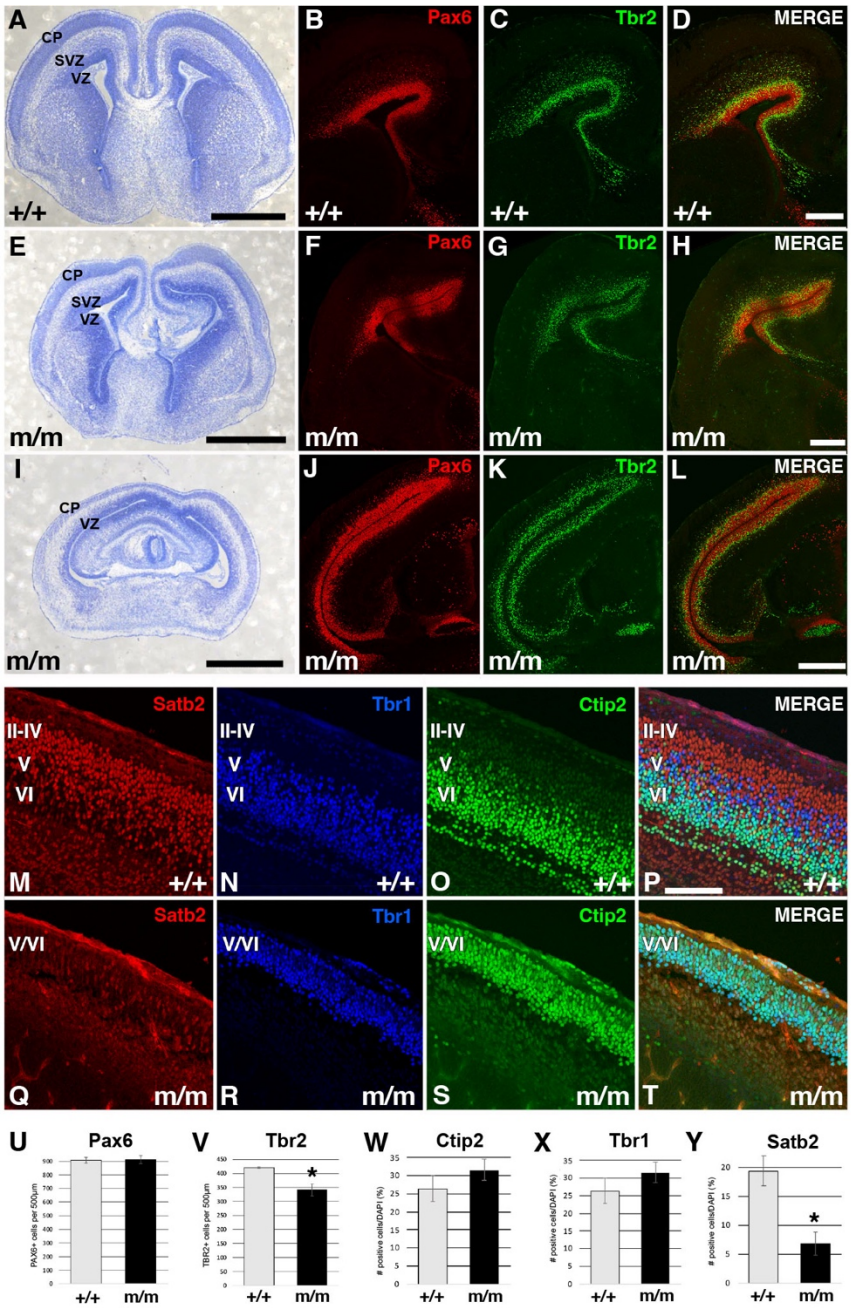

Figure 2. Impaired Cortical Plate Formation with Loss of Tbr2+ Intermediate Progenitors in *Ohia*$^{m/m}$ Mutant Brain

A-L. Sections of the brain of E16.5 control (A-D) and *Ohia*$^{m/m}$ mutant mice with mild (E-H) or severe (I-L) forebrain hypoplasia were stained with cresyl violet (A,E,I) to delineate the brain tissue architecture. Antibody staining was conducted for markers of apical progenitor cells (Pax6, B,F,J), intermediate progenitor cells (Tbr2 in C,G,K), and merged image showing both markers (D,H,L).

M-T. Section of the cortical plate of E16.5 wildtype (M-P) and mutant (Q-T) mouse brain was stained with antibodies to Satb2, marker for cortical layers II-IV (M,Q), Ctip2 for cortical layers V-VI (N,R), and Tbr1 (O,S) for cortical layer VI, and merged image showing all three markers (P,T).
U-Y. Quantification of number of cells stained by Pax6 (U), Tbr2 (V), Ctip2 (W), Tbr1 (X), and Satb2 (Y) in the brain of 5 *Ohia*$^{m/m}$ mutant and 5 littermate controls. P-values calculated by 2-tailed, unpaired t-test.
Scale bars in A-L indicate 500μm. Scale bars in M-T indicate 100μm.

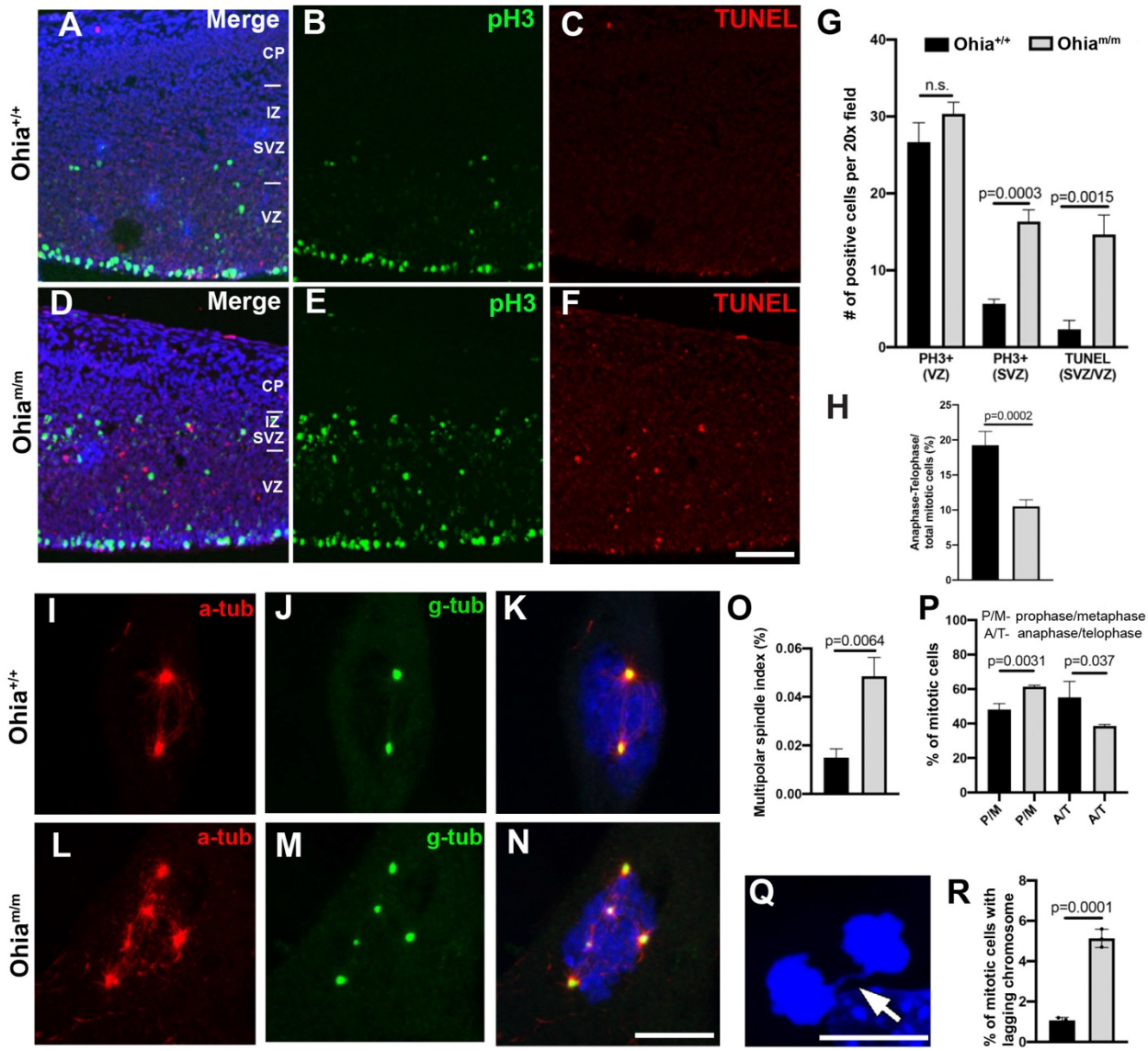

Figure 3. Neural Progenitors in the Cortical Plate Show Mitotic Block With Increase in Cell Death and Possible Role for Multipolar Spindles Indicated by MEF Analysis

A-H. Comparison of the cortex of the brain from E14.5 *Ohia*$^{m/m}$ mutant (D-F) vs. wildtype littermate control embryos (A-C) showed more pH3 and TUNEL staining (G) in the ventricular (VZ) and subventricular (SVC) zones in the mutants. A decrease was also noted in the proportion of mitotic cells in anaphase-telophase (H). P-value obtained using 2-way, unpaired t-test (n=3, *Ohia*$^{m/m}$ mutants, n=3 littermate controls).

I-N. MEFs generated from wildtype (I-K) and *Ohia*$^{m/m}$ mutant embryos (L-N) were immunostained with α-tubulin and γ-tubulin. Mitotic cells in the mutant MEFs showed increase in multipolar spindles (quantification in panel O). MEFs were generated from 3 *Ohia*$^{m/m}$ and 3 littermate control

embryos, with >500 cells analyzed per embryo derived MEF. P-value calculated by 2-way, unpaired t-test.

P-R. *Ohia*$^{m/m}$ MEFs showed reduction in the proportion of mitotic cells in anaphase/telophase (P) and an increase in lagging chromosomes during anaphase (Q,R) P-value obtained using 2-way, unpaired t-test.

CP, cortical plate; IZ, intermediate zone; SVZ, subventricular zone; VZ, ventricular zone; P/M, prophase/metaphase; A/T, anaphase/telophase. Scale bars = 100μm.

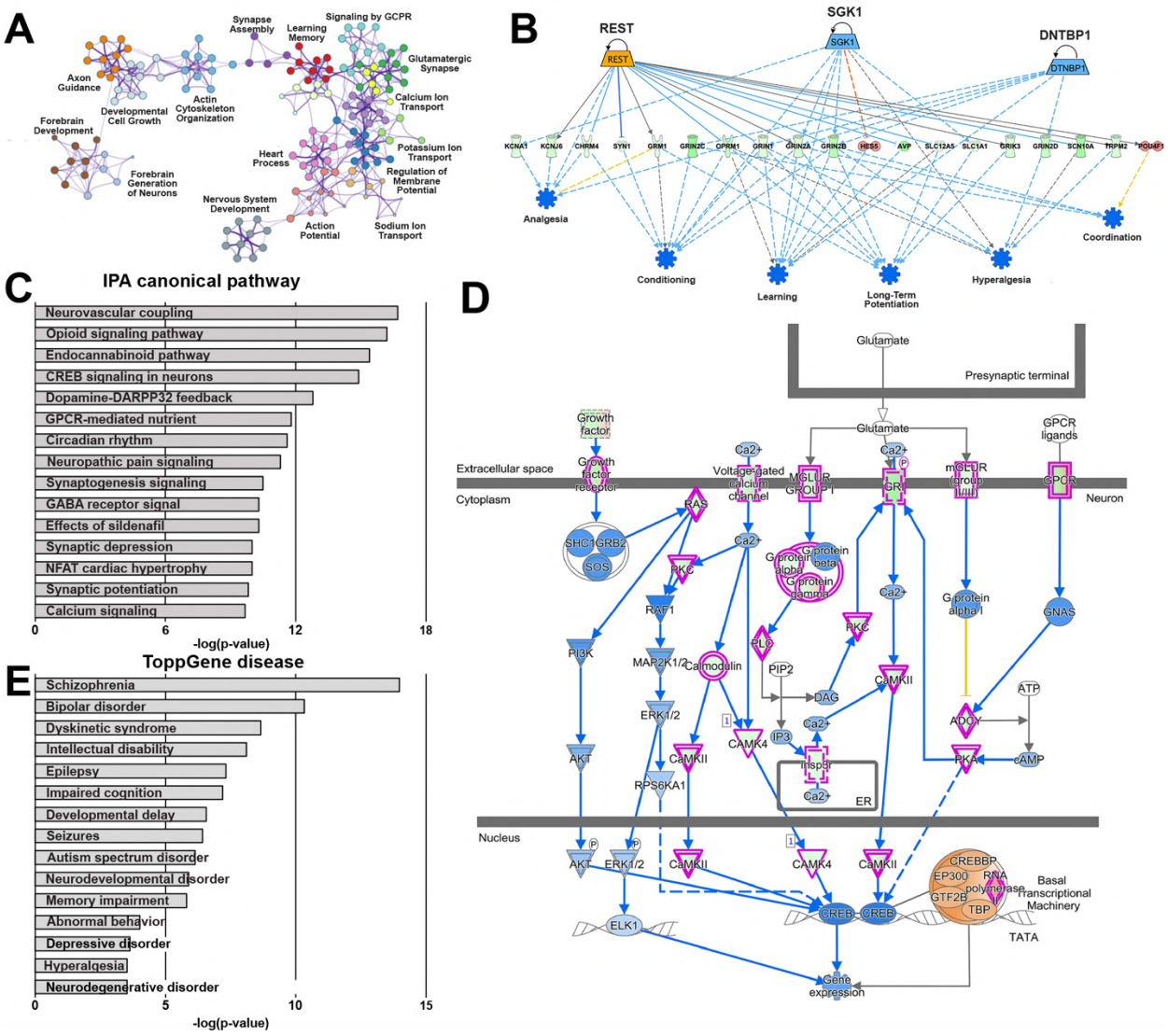

Figure 4. Transcriptome Profiling Shows Dysregulated Neurodevelopment in *Ohia*$^{m/m}$ Mutants

Differentially expressed genes (DEGs) recovered from RNAseq analysis of E14.5 *Ohia* mutant brain were analyzed for pathway enrichment using Metascape (A), Ingenuity Pathway Analysis (IPA) for upstream regulators of downstream neurodevelopmental outcomes (B, red for upregulated, green for downregulated), IPA canonical pathway (C), and IPA curated CREB signaling pathway (D), with purple outline indicating genes found to be differentially expressed, with green fill for downregulated and red fill for upregulated DEGs. (E) Disease terms recovered from ToppGene analysis of recovered DEGs.

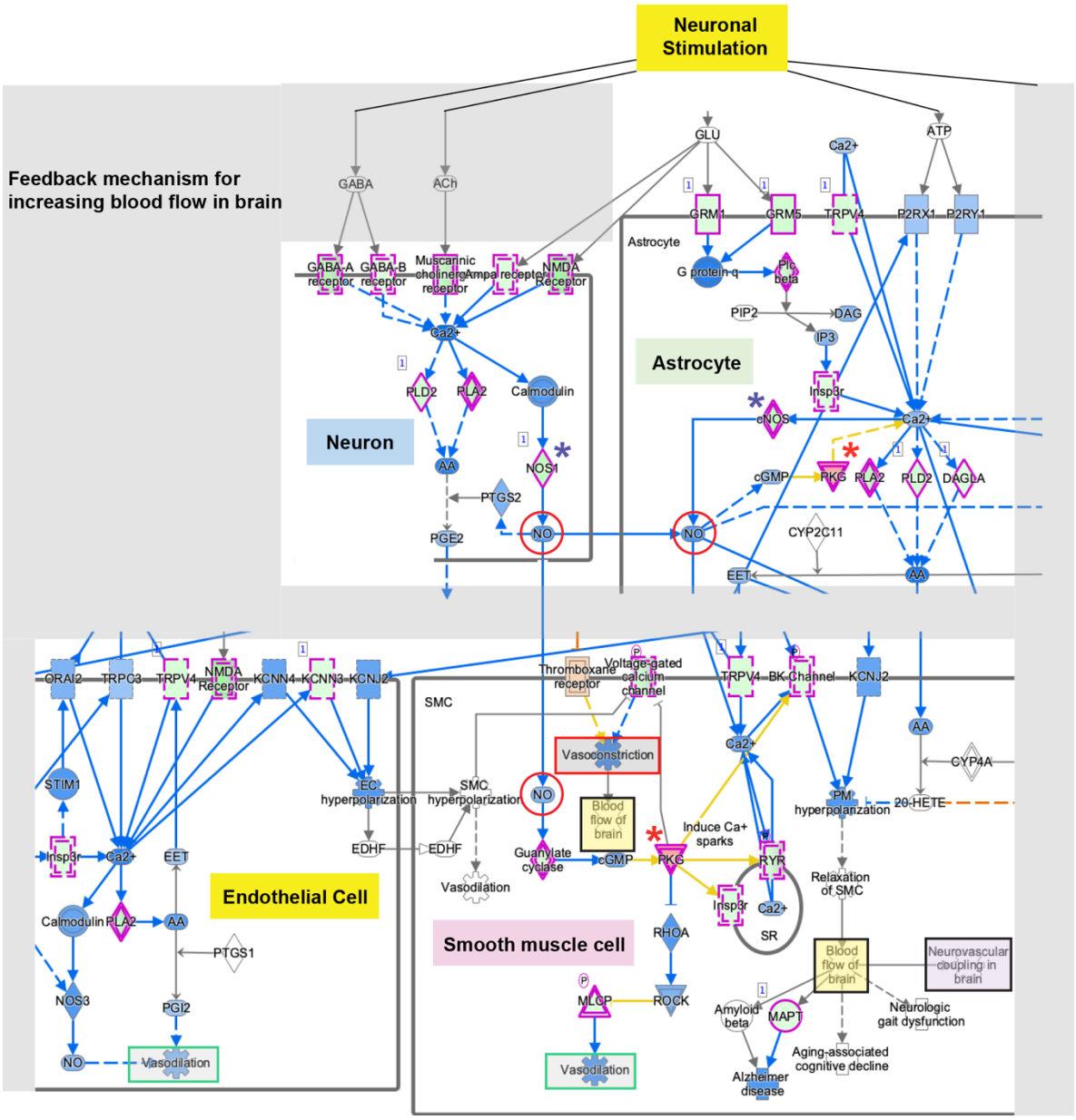

Figure 5. Dysregulated Expression of Genes Associated with Neurovascular Coupling. Modified IPA curated neurovascular coupling pathway illustrating dysregulated expression of genes involved in neurovascular coupling. DEGs identified in *Ohia* brain highlighted in purple outline.

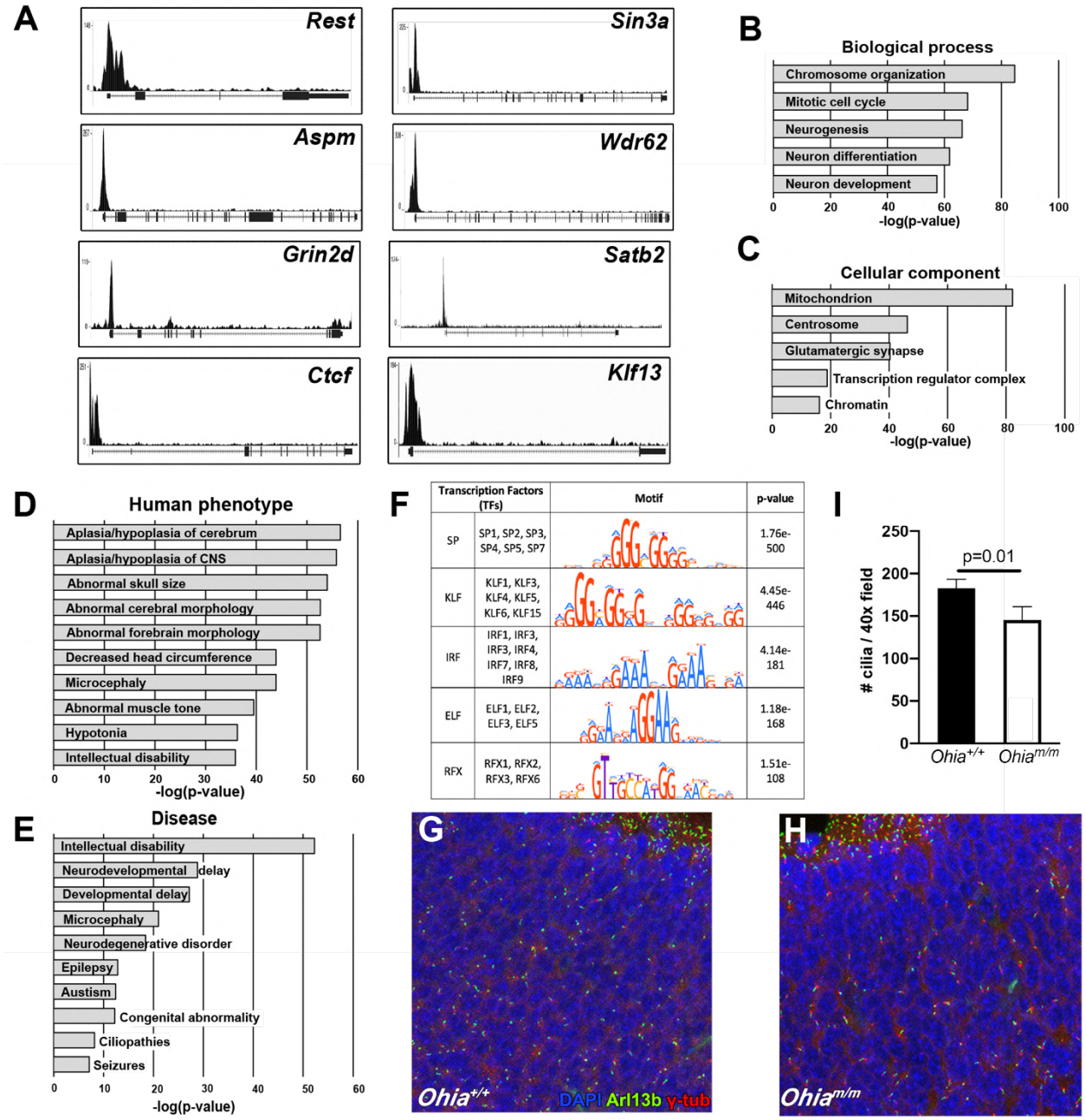

Figure 6. Sap130 Chromatin Immunoprecipitation Sequencing Analysis of Mouse Brain and Examination of Cilia in the *Ohia* Brain Tissue

ChIP-seq analysis of wildtype E14.5 mouse embryo brain was conducted using Sap130 antibody.

A. Sap130 occupancy in the 5' upstream promoter region of selected genes is shown in panel A, including Rest and Sin3A, and two genes associated with microcephaly (*Aspm, Wdr62*).

B-E. Pathways in GO Biological Process (B) and Cellular Components (C), as well as Human Phenotype (D), and Disease (E) terms recovered from ToppGene gene enrichment analysis of Sap130 ChIPseq target genes.

F. Motif enrichment analysis of the Sap130 ChIPseq target genes identified putative Sap130 DNA binding sequences.

G-I. Cilia visualization in sections of wildtype (G) and *Ohia*$^{m/m}$ mutant brain tissue (H) immunostained with Arl13b (cilia, green), γ-tub (centrosome, red) and DAPI. Quantification showed reduction of cilia in the mutant brain (I, n=3 *Ohia* mutant and 4 littermate controls). P value determined by 2-tailed, unpaired t-test.

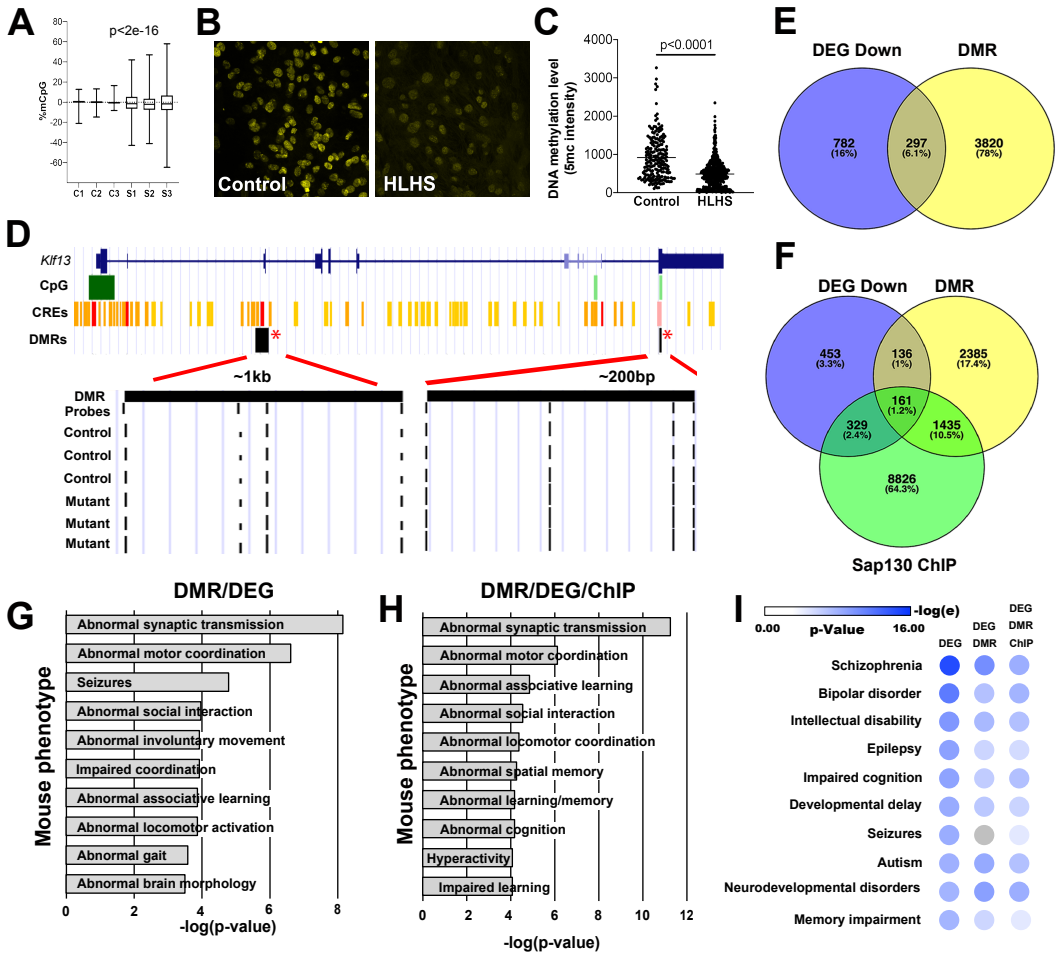

Figure 7. Molecular profiling of *Ohia*$^{m/m}$ brain tissue with integration of genome-wide methylome with RNAseq and Sap130 ChIPseq analyses.

A. Quantification of methyl-CpGs in promoter region of wildtype (n=3, C1, C2, C3) and *Ohia*$^{m/m}$ brain (n=3, S1, S2, S3) tissue revealed reduced DNA methylation in the *Ohia*$^{m/m}$ brain tissue.

B,C. Antibody staining for mCpG in iPSC cardiomyocytes showed less staining in the HLHS patient vs. control iPSC-CM (B). This was confirmed with quantification shown in scatter plot (mean±SEM) for n=200 cells from two control subjects and n=409 cells from four HLHS subjects (C). P-value determined by Mann-Whitney test.

D. Increased methylation of two CpG sites in two DMRS found in *Klf17* (denoted by red asterisk) in the *Ohia*$^{m/m}$ brain tissue.

E,F. Venn diagrams show two-way intersection of downregulated DEGs with genes associated with DMR (E) and three-way intersection of down regulated DEGs, genes associated with DMR, and genes recovered from Sap130 ChiPseq (F).

G, H. ToppGene enrichment analysis for Mouse Phenotypes recovered from the two-way (G) or three-way (H) intersection of the downregulated DEGS with genes associated with DMRs or with DMRs and Sap130 ChIP target genes.

I. Circle plot showing significant Disease association identified by the ToppGene enrichment analysis of the RNAseq recovered down regulated DEGs (first column), genes shared between the down regulated DEGs and DMR associated genes (second column) and the down regulated DEGs, DMR associated genes, and ChIPseq target genes (third column). All three analyses yielded the same Diseases, but with somewhat different p-value ranking as shown by the color coding in the circle plot.

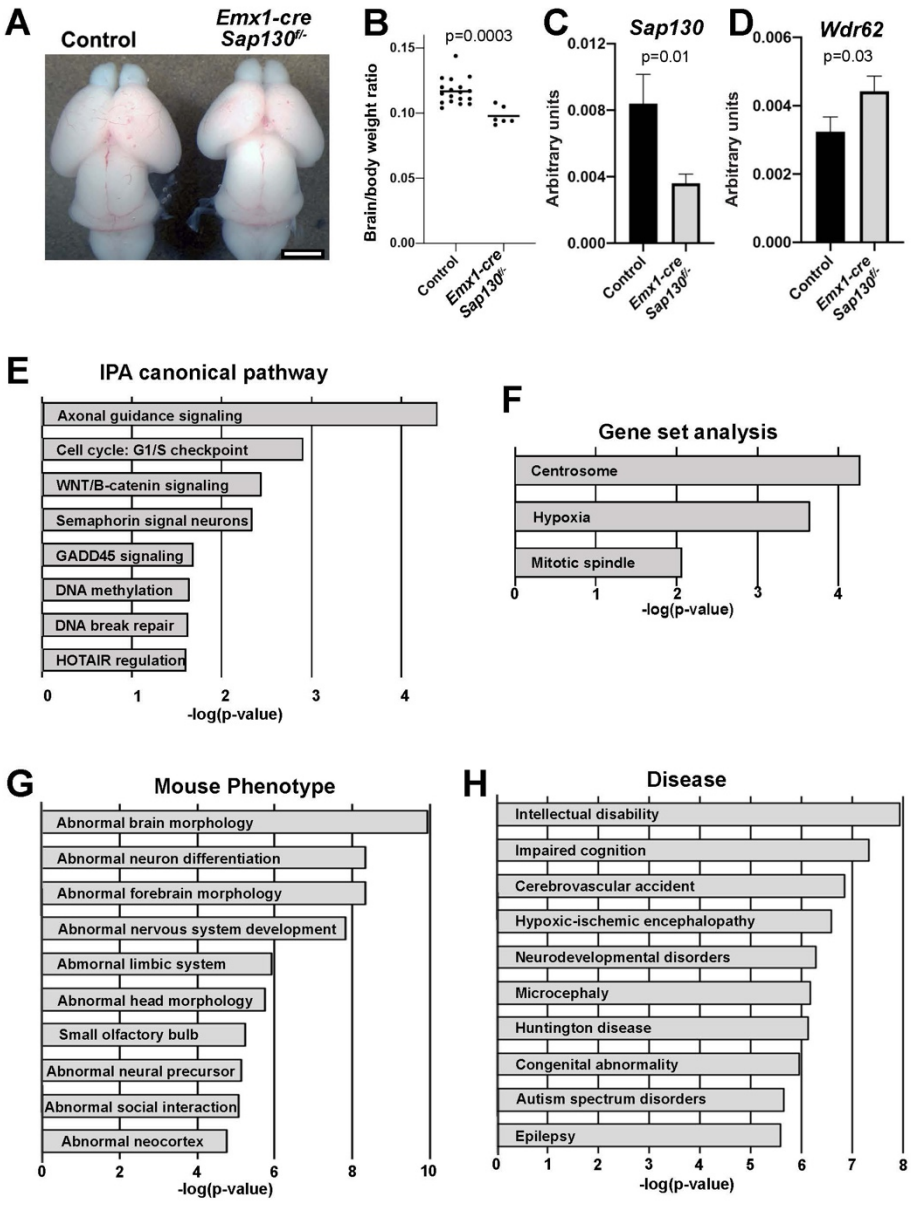

Figure 8. *Emx1-cre Sap130$^{f/-}$* Mice Show Microcephaly With Transcriptome Profiling Showing Abnormal Neurodevelopment

A. Wildtype newborn control (left) and *Emx1-cre Sap130$^{f/-}$* mutant (right) brains.

Scale bar = 500µm.

B. Brain/body weight ratio for newborn control and *Emx1-cre Sap130$^{f/-}$* mice confirm brain hypoplasia in the *Emx1-cre Sap130$^{f/-}$* mice.

C. qPCR of *Sap130* transcripts in E14.5 forebrain tissue from 4 control and 4 *Emx1-cre Sap130$^{f/-}$* mice showed decrease in *Sap130* transcripts, demonstrating efficacy of the Emx1-Cre mediated *Sap130* deletion.

D. qPCR of *Wdr62* transcripts in E14.5 forebrain tissue from 4 control and 4 *Emx1-cre Sap130*$^{f/-}$ mice showed increased transcript expression, indicating possible centrosome amplification.

E-I. IPA and ToppGene analysis of DEGs from RNAseq of E14.5 forebrain tissue from *Emx1-cre Sap130*$^{f/-}$ vs. control mice. Shown are the results obtained with IPA Canonical Pathway (E), IPA Gene Set (G) for hallmark centrosome, hypoxia, and mitotic spindle genes, and ToppGene analysis for Disease (H) and Mouse Phenotype (I).

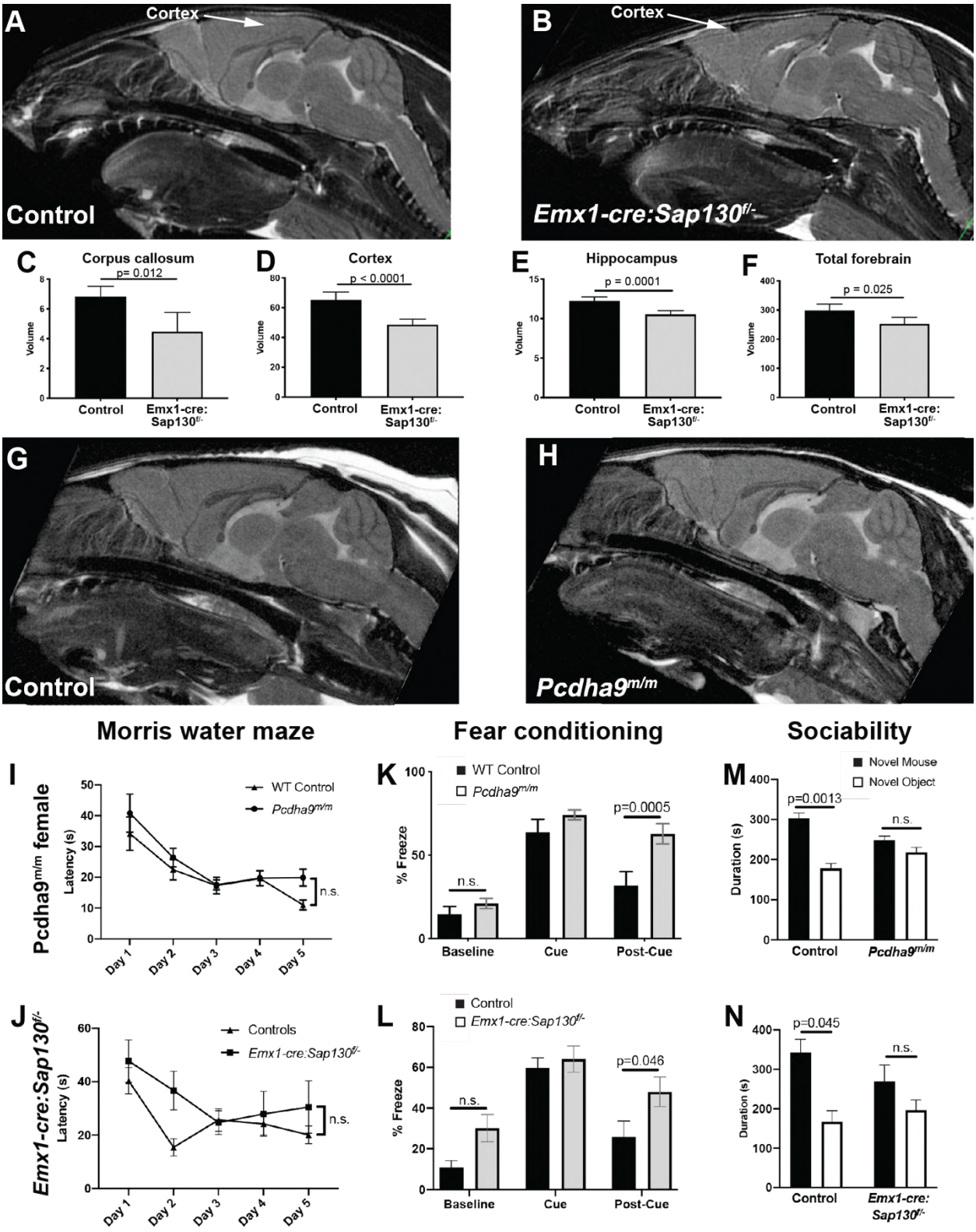

Figure 9. Brain and Behavioral Analysis of *Emx1-cre Sap130$^{f/-}$* and *Pcdha9$^{m/m}$* Adult Mice

A-F. Adult brain MRI of wildtype (A), and *Emx1-cre;Sap130*$^{f/-}$ adult mice (B). Note the marked reduction in size of the cortex. Quantitative analysis showed significant reduction in brain volumes associated with the corpus callous (C), the cerebral cortex (D), the hippocampus (E), and forebrain (F).

G,H. Adult brain MRI of wildtype (A), and *Pcdha9*$^{m/m}$ adult mice (B). No change was observed in anatomical structure of the *Pcdha9*$^{m/m}$ mouse brain.

I-N. Neurobehavioral testing was conducted using three tests: Morris water maze (I,J), cued fear conditioning (K,L), and three chamber sociability test (M,N). In both *Pcdha9*$^{m/m}$ female mice and *Emx1-cre:Sap130*$^{f/-}$ mice, significant deficits were observed for fear conditioning and sociability, but no difference was observed in the Morris water maze. Similar analysis of *Pcdha9*$^{m/m}$ male mice showed no change relative to wildtype control male mice (Supplemental Figure S7). Morris water maze analyzed by 2-way repeated measures ANOVA, fear conditioning analyzed by 2-way repeated measures ANOVA, and sociability tested analyzed by two-way and three-way ANOVA.